Regional Geophysical–Geological Zonation

4

The regional geological–geophysical zonation may be subdivided into: (1) the development of new geophysical maps (cross sections) for the region under study, (2) qualitative and semiquantitative analysis of geophysical data (including different schemes of geophysical data processing and transformation), (3) quantitative analysis of geophysical anomalies (inverse solution) and preliminary regioning, and (4) compilation of final geophysical–geological maps. Let us successively consider these stages with application to the territory of Azerbaijan.

4.1 Development of New Geophysical Maps (Cross Sections)

4.1.1 Gravity Field

The development of novel exact geophysical maps (cross sections) basing on new obtained data and reinterpretation of some old data is of great importance. A bright example of such new map compilation is the development of new Bouguer gravity map of the Caspian Sea and adjacent areas (Lodzhevsky and Kadirov 2001) (Fig. 4.1). This gravity map was constructed on the basis of Dehghani and Makris (1983), Gravity map of the USSR (1990), and Kadirov (2000a).

The gravity map is characterized by anomalies of various geometries and amplitudes. The anomaly field of the northern part of the basin is represented by the area of increased horizontal gradients subparallel to the strike of the Caucasus. In the northwestern part of the SCB, there is a vast gravity minimum with amplitude reaching 125 mGal. The central part of the basin is represented by a gravity minimum and by an isometric maximum of the gravity field in the southwest and in the southeast (Safidrud and Godin uplift). The area of increased gradients from the Alborz mountains to the south up to the deepwater part of the basin is typical for the southern part of the SCB. The area of the Central Alborz is characterized by a negative anomaly (−120 mGal) (Kadirov and Gadirov 2014).

4.1.2 Remote Sensing

Today, the origin and evolution of the Caucasus are mainly explained in terms of plate tectonics (e.g., Khain and Ryabukhin 2002). In a brief review, Kopf et al. (2003) noted that the present-day Caucasus is dominated by thrust faulting due to continental collision. From the Jurassic to the Paleogenic eras, subduction of the Tethyan seafloor occurred along the southern margin of the Turkish and Iranian blocks, resulting in calc-alkaline arc volcanism and a wide back-arc basin system. The spread of the Red Sea began during the Early Miocene, and the Arabian Plate migrated northward, accompanied by a reduction in width of the Tethys. After its closure (~20 Ma), subduction shifted to the north. As a result of the indentation of the Arabian block, the continuous back-arc basin was separated, and the oceanic crust only remained in the Black Sea and the southern Caspian Sea. The continuous northward drift of the Anatolian Plate led to initial continental collision expressed by the formation of the Lesser Caucasus and the subsequent resurrection of the Greater Caucasus during the Middle Pliocene. Currently, continental convergence continues at a rate of up to ~20–30 mm/year (e.g., Reilinger et al. 2006) along strike-slip faults, where most of the modern tectonic activity is localized (Fig. 4.2). Reilinger et al. (2006) note the tendency for motion rates to increase from west to east along strike of the Main Caucasus thrust (MCT) (≈120° azimuth). Besides this, there is little change in the magnitude of velocity estimates across the Lesser Caucasus along transects perpendicular to the Caucasus range. Taking into account the low level of seismic activity within the Lesser Caucasus, Reilinger et al. (2006) propose to imply block-like, counterclockwise rotation of the Lesser Caucasus resulting in increased convergence from west to east along the MCT.

Without hesitation, the GPS data constructions (e.g., Reilinger et al. 2006; Kadirov et al. 2008) must be coordinated with other remote sensing data or regional geophysical field distribution. For example, the map of deep-seated lineaments (Fig. 4.3) (which is undeservedly little used) shows very interesting tectonic patterns for Azerbaijan and adjacent

A.A. Alizadeh et al., *Geosciences of Azerbaijan*,
Regional Geology Reviews, DOI 10.1007/978-3-319-40493-6_4

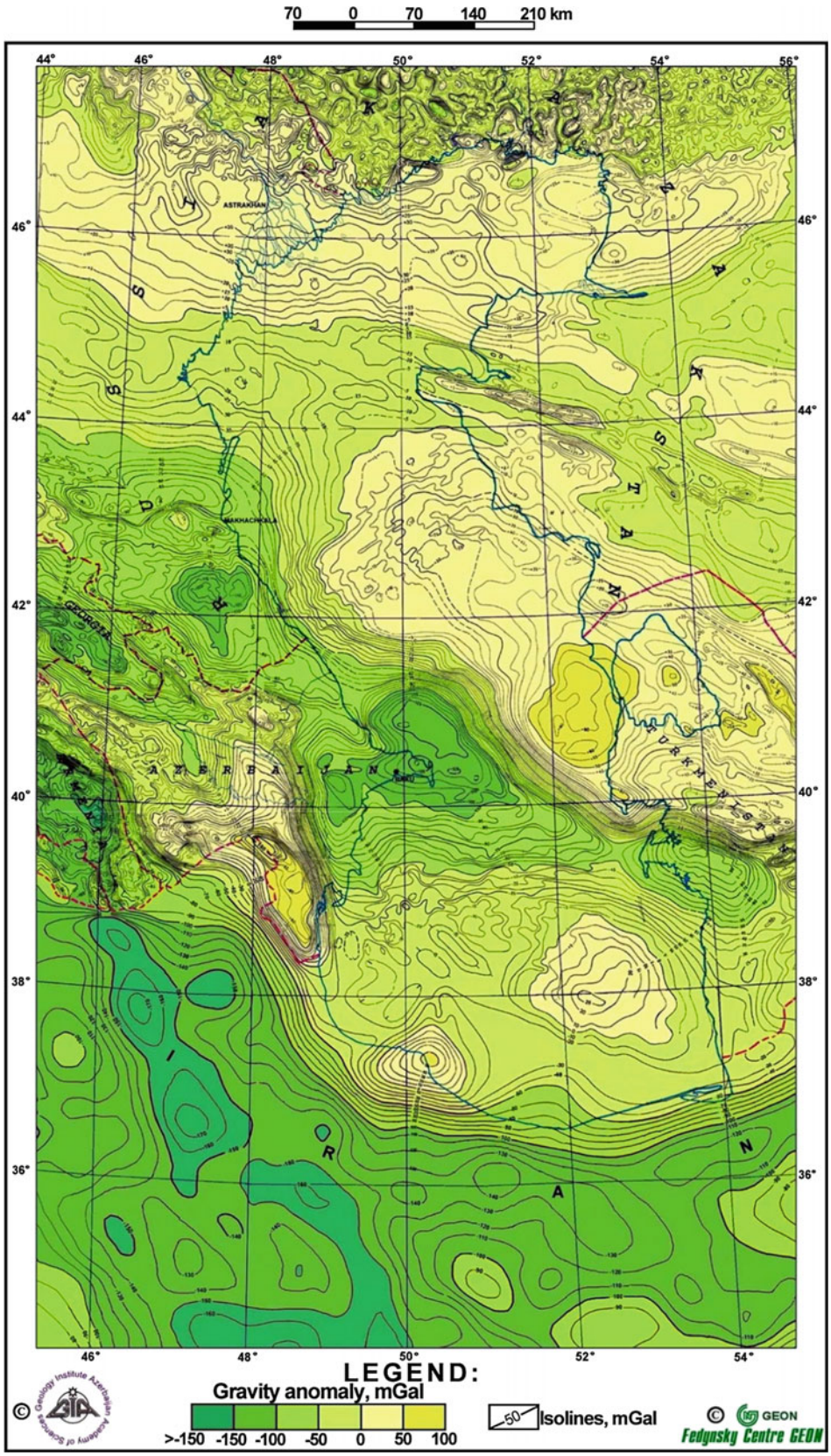

Fig. 4.1 Caspian region: Bouguer gravity map (Lodzhevsky and Kadirov 2001)

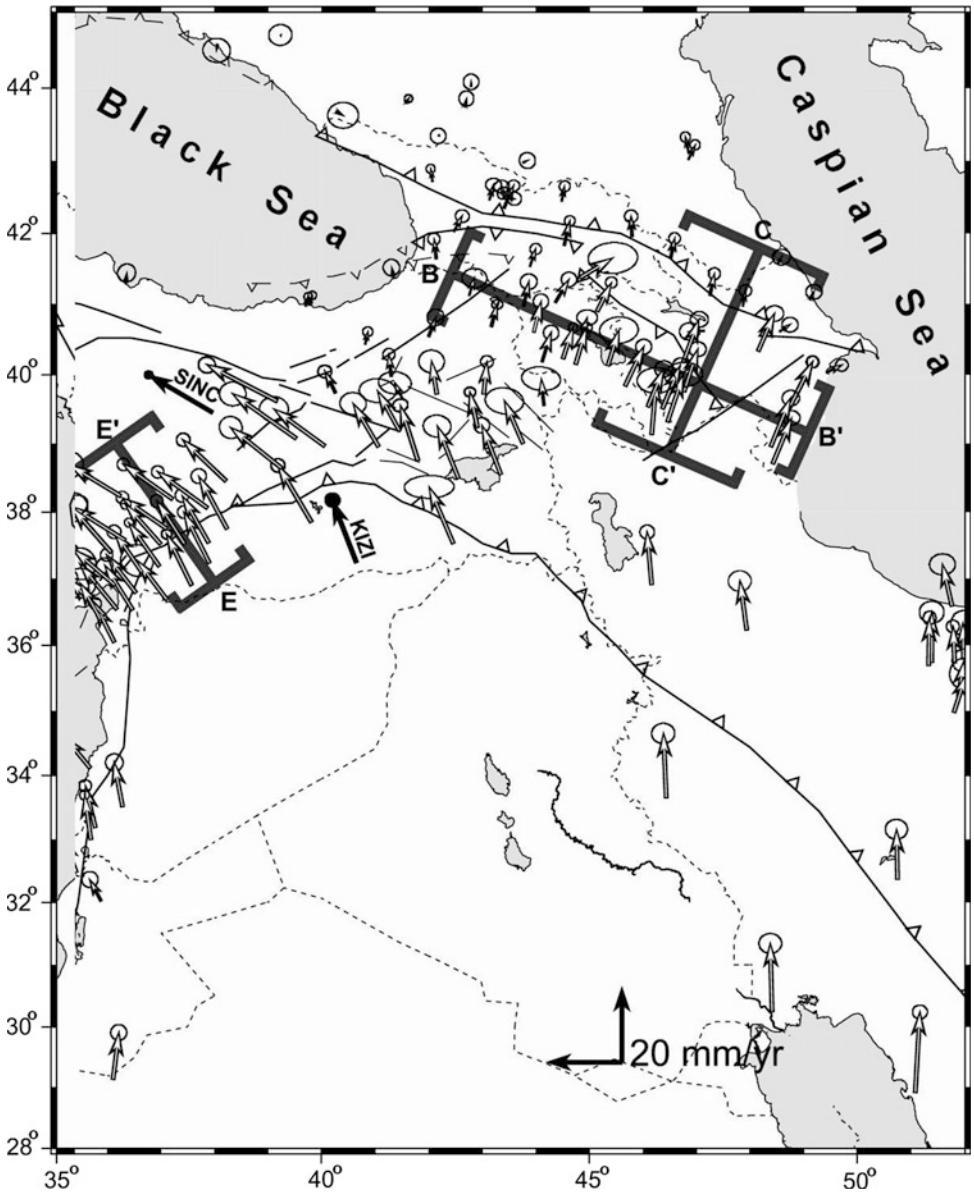

Fig. 4.2 Map showing GPS velocities with respect to Eurasia Locations and widths (*brackets*) of velocity profiles along and across strike of the Greater Caucasus (B′–B, and C′–C, respectively), the eastern Anatolian fault (E–E′) (fragment of Fig. 3 from Reilinger et al. (2006), with minor modifications)

regions. Besides other peculiarities, the intersection of deep faults was detected at the northern point of sharp tectonic wedge where the destructive Spitak earthquake of 1988 (coordinates: 40°49′ N, 44°15′ E) took place.

Gadjiev et al. (1989) identified this feature from this map of the Caucasus (Fig. 4.3) by calculating the lithospheric heterogeneity at different depths. The sum total length of the lineaments within square cells with different sides (corresponding to cubic blocks of different depths) served as a measure of heterogeneity (Khesin et al. 1996).

Note that this map of the deep structure of the Caucasian lithosphere (Fig. 4.3) is consistent with the depiction of horizontal gradients of isostatic and lithospheric gravity anomalies shown in Fig. 4.4.

Figure 4.5 illustrates more detailed example—the relation between hydrocarbon accumulations in the Kur basin and regional faults (faults location was obtained from Landsat data analysis). The map shows many faults with different orientations and styles of movement (sublatitudinal, Caucasian, anti-Caucasian, submeridianal, etc.) and depths of occurrence (from pre-Mesozoic to the younger Cenozoic). These findings were used to examine the fault systems and oil and gas content in Eastern Azerbaijan (Zeynalov 2000).

4.1.3 Thermal Field

Geothermally, Azerbaijan is one of the most investigated regions of the world (e.g., Mekhtiyev et al. 1960, 1971; Sukharev et al. 1969; Yakubov and Atakishiyev 1973; Lebedev and Tomara 1981; Aliyev 1988; Kerimov et al. 1989; Aliyev and Aliyev 1995; Pilchin and Eppelbaum

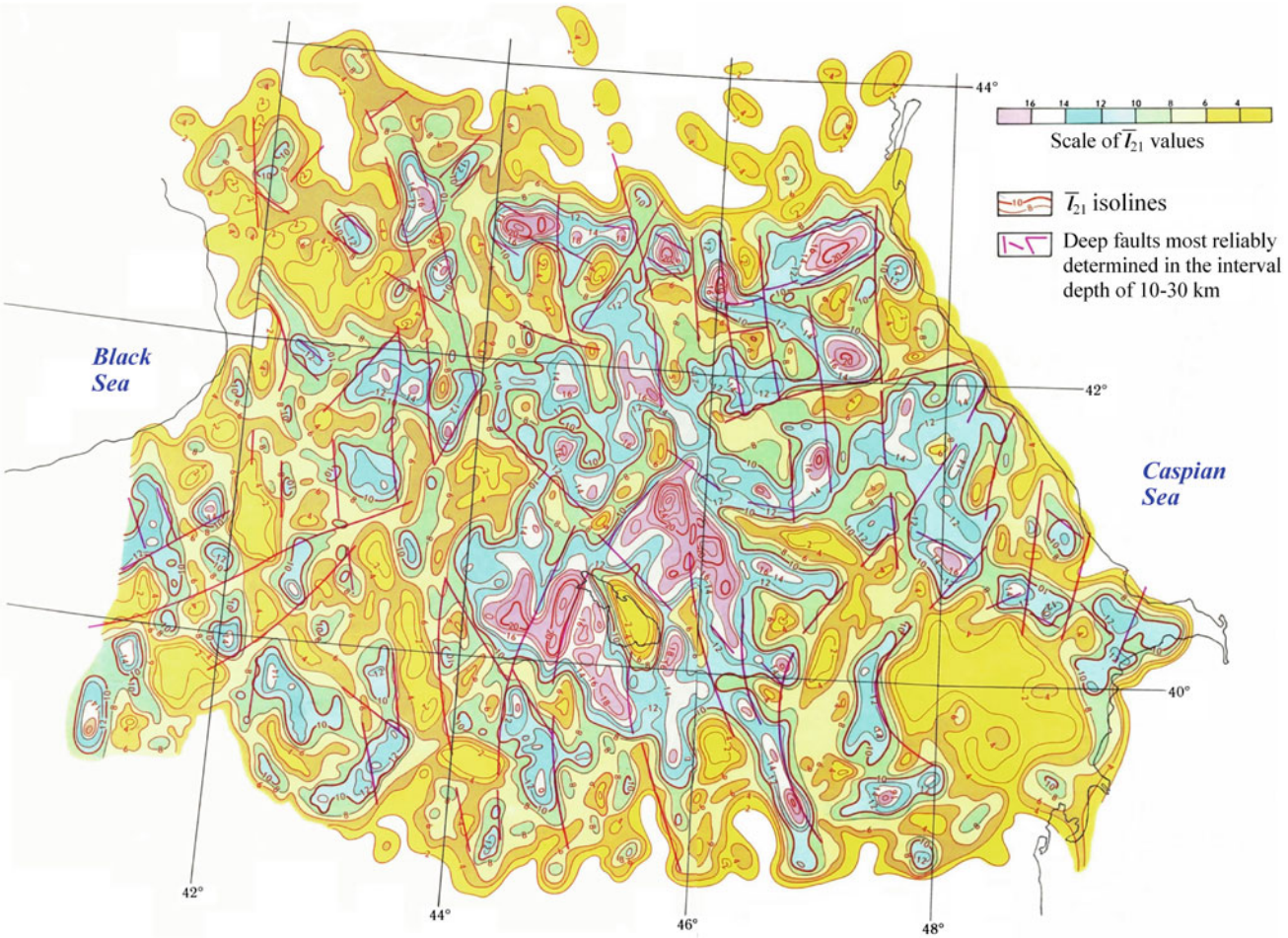

Fig. 4.3 Deep structure of Azerbaijan and adjacent regions (the cut at ≈10 km in depth) according to the satellite data analysis (after Gadjiev et al. 1989)

1997; Aliyev and Mukhtarov 2000; Rustamov 2001; Aliyev et al. 2005a, b; Mekhtiyev et al. 2003; Mukhtarov 2004, 2011, 2012; and Eppelbaum et al. 2014).

The many year's results of heat flow measurements on the territory of Azerbaijan are generalized in Fig. 4.6. This map is of great interest not only for studying deep structure and geological–geophysical mapping, but also for searching economic minerals (first of all, hydrocarbons) in this region.

Comparison of vertical and horizontal geothermal gradients at depths of 0–4 km and 0–6 km is shown in Figs. 4.7 and 4.8, respectively.

4.1.4 Radioactivity

Numerous radioactive measurements have been carried out in the territory of Azerbaijan (e.g., Ch. Aliyev and Zolotovitskaya 1996, 2000; Ch. Aliyev et al. 2001; Zolotovitskaya 2003; Ch. Aliyev and Zolotovitskaya 2005; and Ch. Aliyev et al. 2012) (see also Chap. 9 of this Volume).

The study of the radon concentration (anomalies) presents a special interest not only from the environmental point of view.

Considering the impact of other geological factors on the distribution of radon, it is necessary to note that radon is an admixture component and is emitted from the subsoil to the surface in hydrocarbon, nitrogen, and carbon dioxide gas flows. Prevalent pathways of vertical (subvertical) migrations are high-permeable zones of deep faults that usually are expressed by high thermal flows. Taking that into account, the radon distribution map was compared with deep faults and earthquake epicenters in Azerbaijan area (Fig. 4.9) and with a map of temperature distribution at 5000 m depth (Mukhtarov 2011). This comparison reveals a correlation of studied parameters confirming theoretical and some lateral assumptions (Ch. Aliyev et al. 2012).

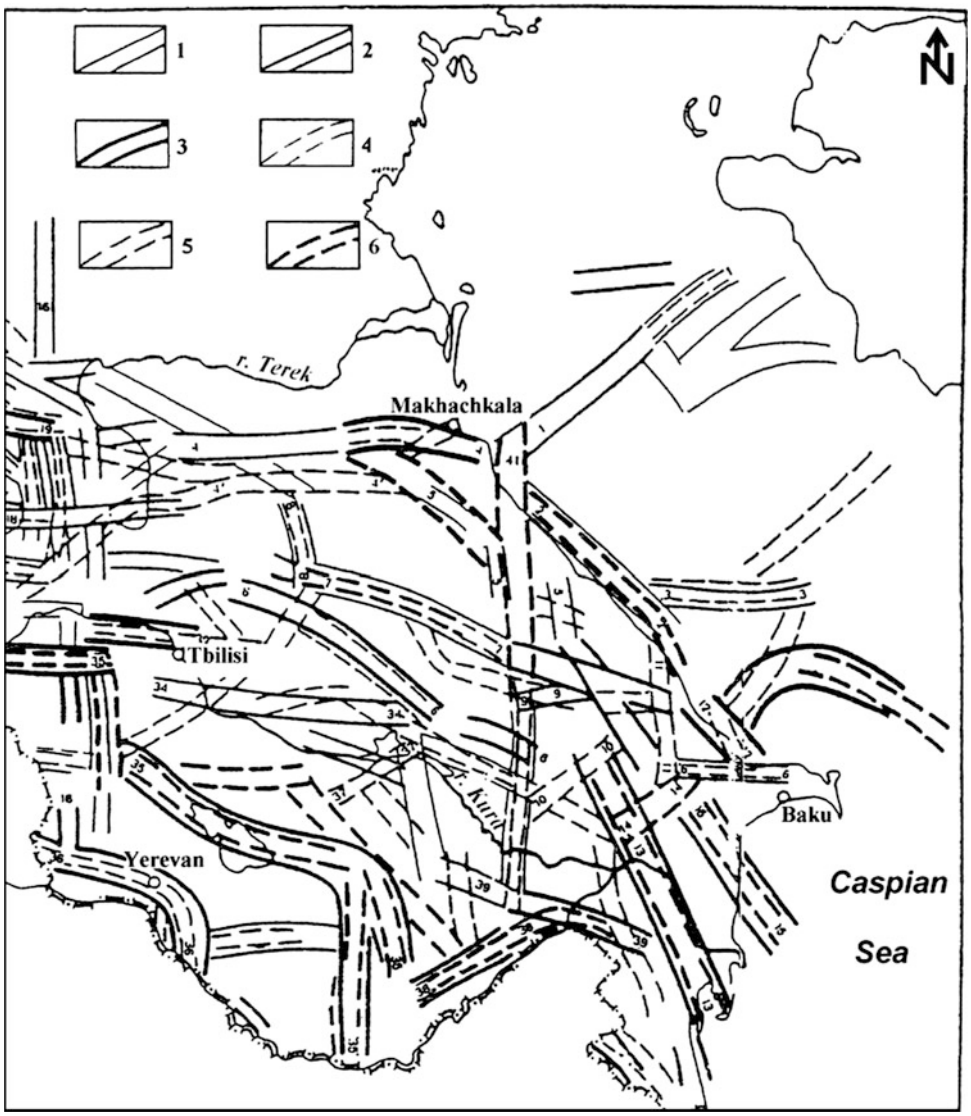

Fig. 4.4 Diagram of horizontal gradients of isostatic and lithospheric gravity anomalies (after Gorshkov and Niauri 1984, with small modifications). Zones of horizontal gradients of isostatic anomalies in mGal/km: (*1*) 0.5–1, (*2*) 1–2, (*3*) 3, zones of horizontal gradients of lithosperic anomalies in mGal/km: (*4*) 0.5–1, (*5*) 1–2, (*6*) 2

4.1.5 Paleomagnetic Analysis

Paleomagnetic data are an important source for paleotectonic reconstructions (e.g., Gorodnitsky et al. 1978; Tauxe et al. 2009). It should be noted that some geodynamic and tectonic problems cannot be solved by any other geophysical or geological method (Eppelbaum and Katz 2015). The reduction of the location of the magnetic pole for different terranes at different times can serve to evaluate regional rotation and the relative displacement of these terranes. Issayeva and Khalafly (2006) carried out an important paleomagnetic study of this type. It was revealed that the regions of the Lesser and Greater Caucasus and Iran rotate clockwise through about 20–30° with respect to the magnetic meridian, and the North Anatolia rotates anticlockwise through about 30–40° (Fig. 4.10).

The average coordinates of the paleomagnetic poles for Azerbaijan, Georgia, Armenia, Turkey, and Iran were compared to the Russian Platform and showed that these regions have been connected to the Eurasian continent since the Upper Eocene. The Lesser Caucasus has moved 5–7° to the south with respect to the Eurasian continent.

4.1.6 Deep Seismic Sounding Reinterpretation

Examples of the deep seismic sounding (DSS) reinterpretation for two DSS profiles crossing Azerbaijan are shown in Chap. 5 (Figs. 5.1, 5.2, and 5.3) (Pavlenkova 2012). Besides this, Chaps. 5 and 6 contain other seismic profiles crossing the Kur Depression and South Caspian basin.

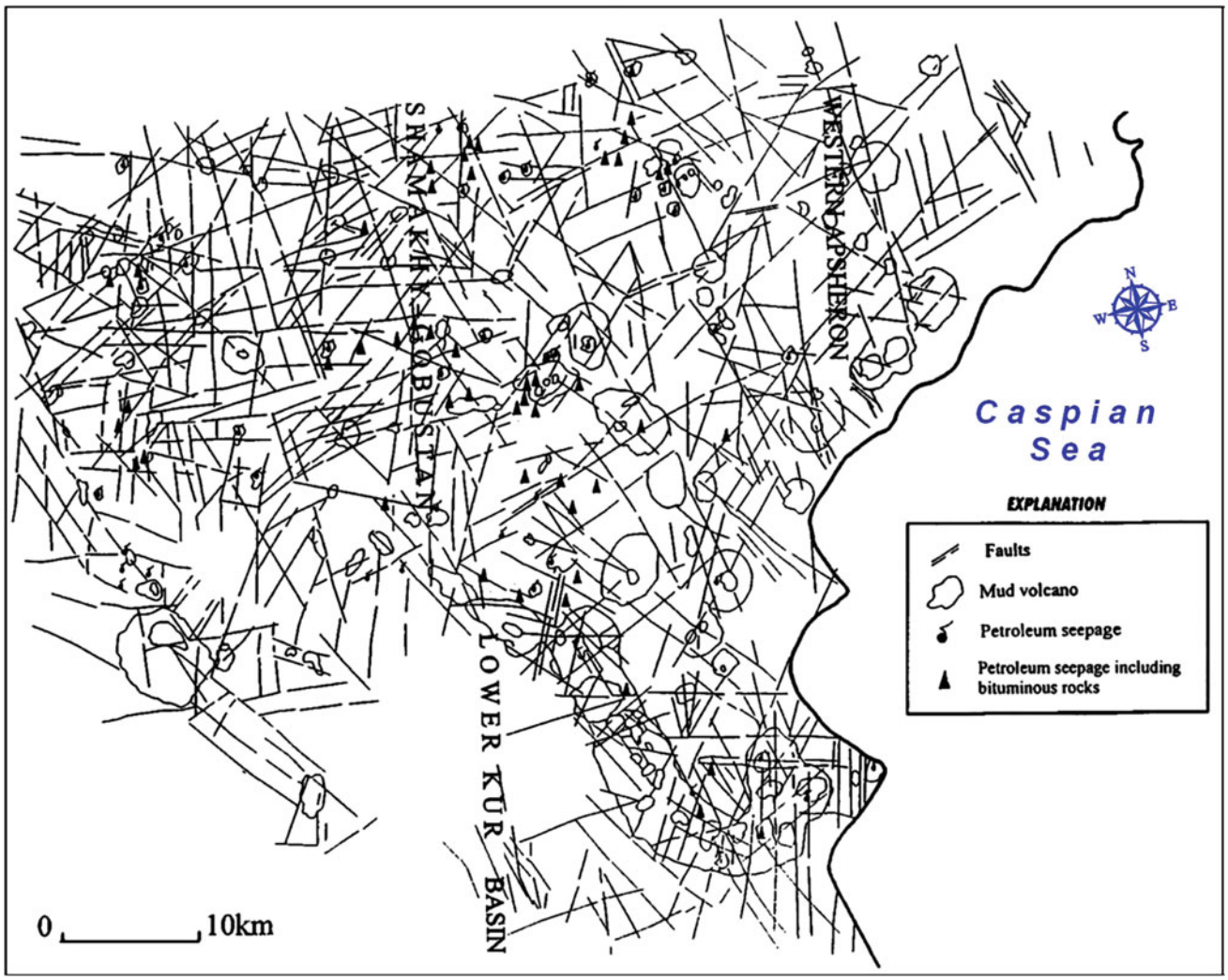

Fig. 4.5 Map of faults from analysis of Landsat data for central-eastern Azerbaijan (after Zeynalov (2000), with minor modifications)

4.2 Qualitative and Semiquantitative Analysis of Geophysical Data

The calculation techniques should be decided upon when developing the initial model of the medium. After the fieldwork is completed, the set of interpretation techniques can be corrected as a function of the particular types of anomalies that were observed. This set of calculations includes techniques to obtain the parameters of a certain class of model bodies typical to the area under survey. The techniques should meet the following criteria: applicability to the specific conditions of the geophysical investigation, in particular under the oblique polarization and rugged terrain relief characteristic of open areas in central and low latitudes, independence of the normal background level, and the choice of the origin of coordinates. The optimal techniques are those which can successfully obtain the above-mentioned parameters. Of special interest is the geophysical field interactive modeling (e.g., Kadirov 2000a; Eppelbaum and Khesin 2012).

The parameters should be determined using a combination of techniques, so that independent data on the parameter values can be obtained. When the 2D condition is satisfied, the calculations should ideally be carried out along a series of profiles in the mid-portion of the anomaly, where the field isolines are nearly parallel. The results should then be averaged. This will ensure higher validity in determining the parameter values.

To obtain the anomalous body parameters, the first stage involves interpolation selection methods (the method of characteristic points, the tangent method, the areas method, etc.). These make it possible to obtain a large number of parameters in a fairly simple way. The next stage involves the methods of singular points and analytical continuation,

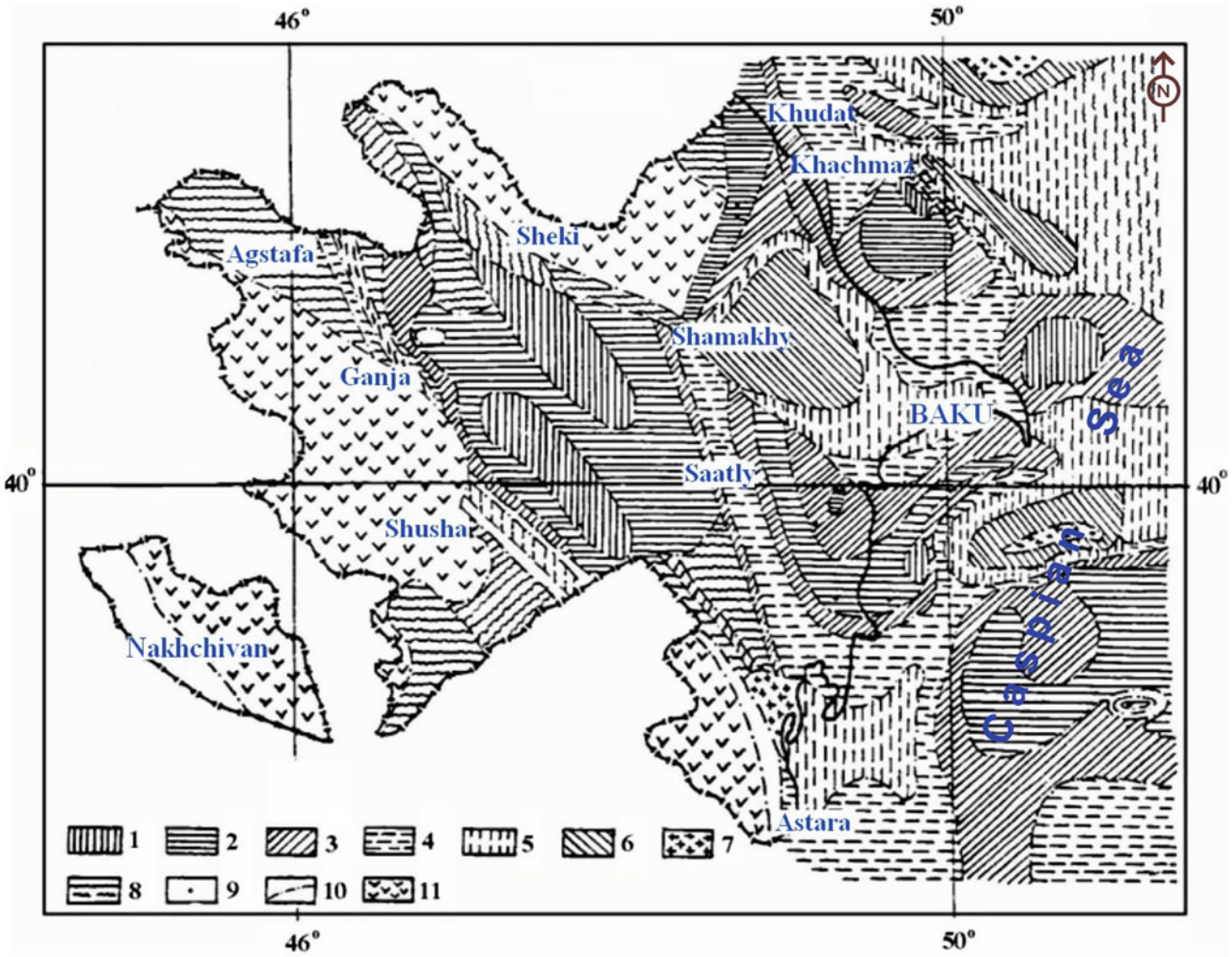

Fig. 4.6 Sketch map of heat flow of Azerbaijan. Heat flow in mW/m^2: (*1*) 0–29; (*2*) 20–30; (*3*) 30–40; (*4*) 40–50; (*5*) 50–70; (*6*) 70–90; (*7*) 90 and higher; (*8*) uncertain; (*9*) heat flow measurement points; (*10*) heat flow zone boundaries; and (*11*) folded mountain structures (Aliyev and Aliyev 1995)

because by this time, the researcher already has the necessary information about the quantitative characteristics of the object. Comparing the results obtained by the methods of interpolation selection to those obtained through the method of singular points will yield a more reliable and valid classification of singular points. The same applies to the method of analytical continuation. In this case, because the range of the upper edge occurrence depth is known, one can avoid the risk of field continuation into the vicinity of the sources.

The selection methods are used at the final stage of (Khesin et al. 1993), when a sufficient amount of data on the object parameters has been acquired. These data enable important corrections and modifications in the initial medium model, thus forming an initial approximation to make the selection: the better the initial approximation, the faster the selection.

The initial approximation involves tracing the average parameters obtained by the above techniques onto the section (scheme) plotted when developing the initial model of the medium with previous data. The information on the sources' shapes and dimensions provides a rationale for selecting the type of approximating expression. The mean-square divergence in the parameters, with prior information and fieldwork experience taken into account, is used to impose constraints on the range of possible values of the parameters.

4.2.1 Magnetic Data Analysis

It is valuable to compare the average parameters obtained by a statistical approach to the results of a deterministic

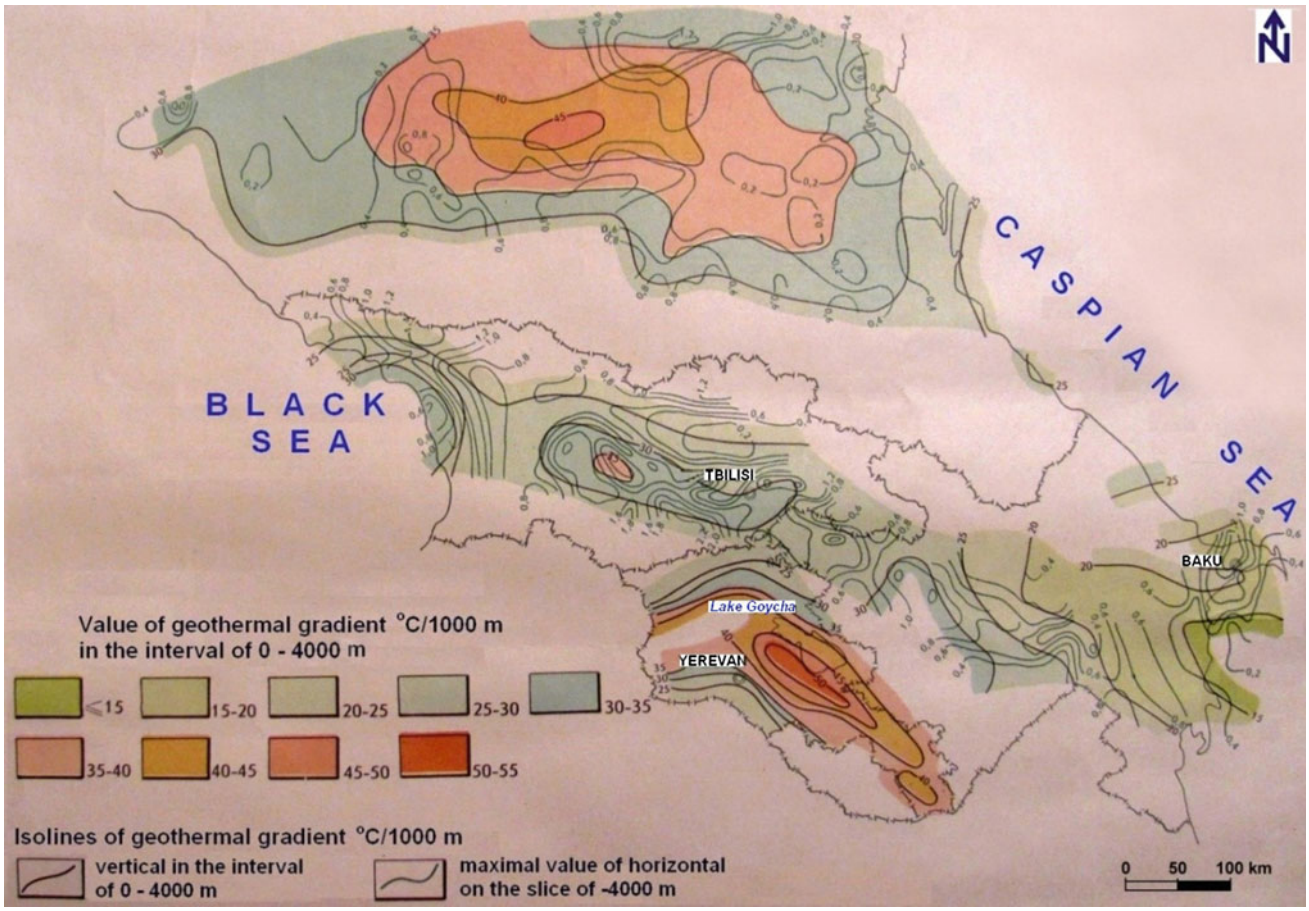

Fig. 4.7 Values of vertical and horizontal geothermal gradients at depths of 0–4000 m in the Caucasian region (after Kerimov et al. 1989)

interpretation. The technique worked out by Klushin and Tolstikhin (1961) estimates the average occurrence depth of magnetized masses by computing the normalized autocorrelation function $R_n(\tau)$ of a field with sources represented by a set of thin vertical beds. The average depth of the upper edge of magnetized sources was calculated by the following formula:

$$\bar{h} = \frac{1}{\pi}\int_0^\infty R_n(\tau)\mathrm{d}\tau = \frac{\tau_e}{\pi}, \tag{4.1}$$

where $\tau_e$is the autocorrelation radius.

We obtained $\bar{h}$ value of 4.3 km which is close to the average depth of the magnetic field's singular points. This technique was applied to the meridional profile through Western Azerbaijan (Fig. 4.11) and confirmed Paffenholtz's (1959) geological concepts.

The rugged relief in Azerbaijan means that various methods should be used to estimate different heights of geophysical field observations. The topographic mass attraction may be of no use, for example, for magnetic investigations directed at singling out a magnetized body among non-magnetic host rocks or for electric exploration to locate conducting ores in a high-resistance medium. In any case, however, the distorting effect of a non-horizontal observation line takes place when the object differs from the host medium by contrasting properties and causes an anomalous vertical gradient.

It is well known that for the purpose of estimating the usefulness of reduction to the common level, the degree of anomaly distortion can be approximated from the formula for any component of the recorded field

$$\Delta U = \frac{\partial U}{\partial z}\Delta H, \tag{4.2}$$

where $\partial U/\partial z$ is the vertical derivative of the field, and ΔH is the relative elevation of the flight height (observation line), i.e., the terrain clearance of the aerial survey.

In aerial surveys along sinuous (in the vertical plane) routes and ground surveys, the sinuosity effect, i.e., reducing observations to horizontal or inclined planes, is theoretically necessary. It substantiates the solution to certain problems associated with quantitative determination of anomalous body parameters in that neglecting the effect of variation in

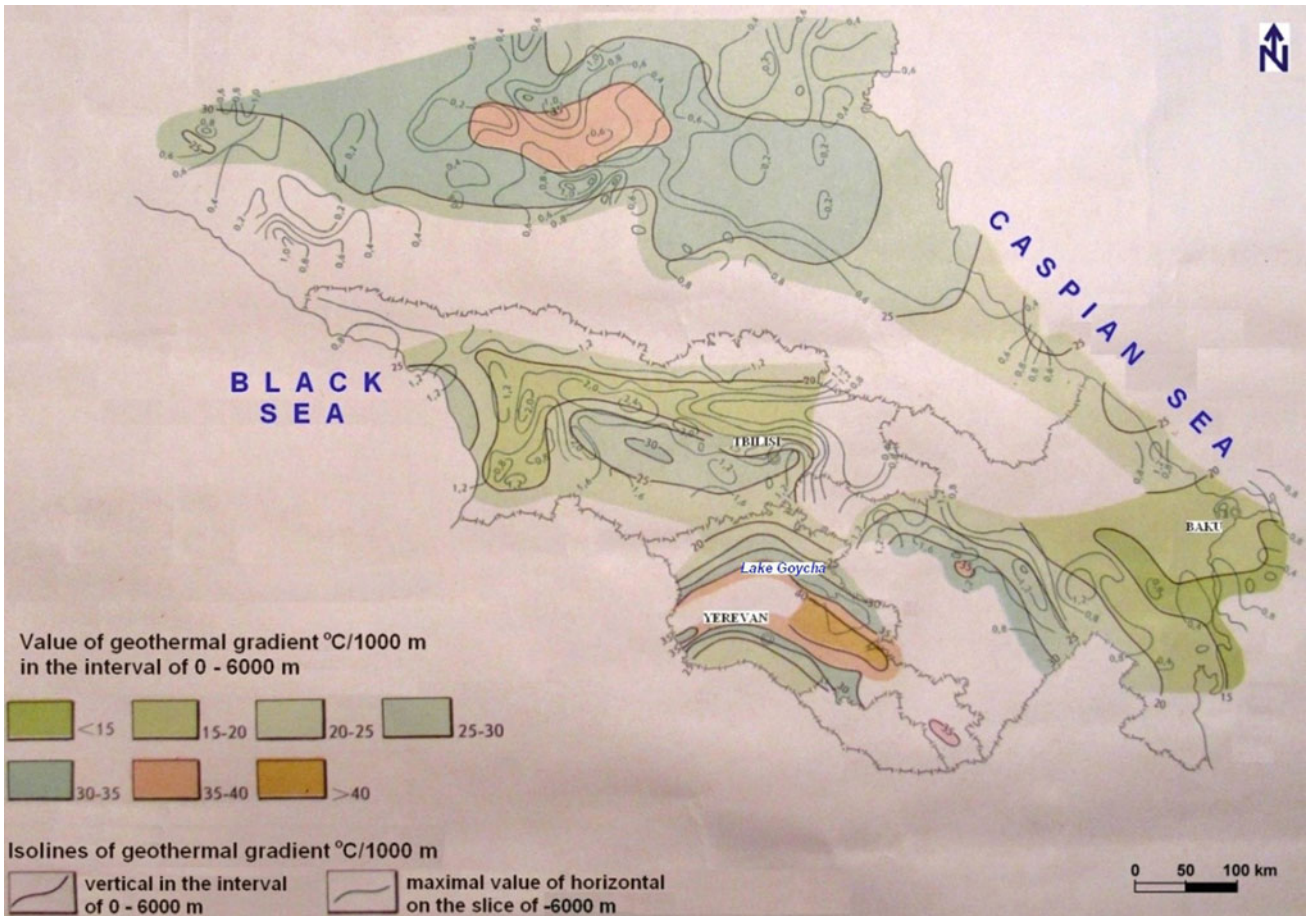

Fig. 4.8 Values of vertical and horizontal geothermal gradients at depths of 0–6000 m in the Caucasian region (after Kerimov et al. 1989)

the observation point heights may introduce errors into the interpretation. Hence, the reduction level should be as close to the acting masses as possible, and if required, several levels should be selected.

Within areas in which the surface profiles have close inclination angles, distortions of the field and its transforms due to the relief also occur. This means there is no need to carry out reduction to the plane if the preliminary regioning of the main forms has determined the dominant dips of the routes.

Subsequent analysis of the field and its transforms should be executed independently within the singled-out areas. Note that the results relate to fictitious bodies of identical forms, and the sizes are similar to those of the real anomalous bodies (Khesin et al. 1996). The evidence shows that the positions of fictitious and real bodies in plane do not differ greatly (max. 0.4 of body depth for a relief dip angle up to 30°). This is not essential for shallow-seated objects. When the relief is very complex in certain plots, it may be necessary to reduce the field to the plane, which should be inclined and as close as possible to the relief.

A general case of the complexity of the physical properties and the geophysical anomaly polygon distribution can be found in the Caucasus. Take for example the magnetic anomaly distribution in the Lok-Garabagh (Somkhit-Agdam) tectonic–magmatic zone of the Lesser Caucasus (Fig. 4.12).

Even within the limits of this zone, the magnetic anomaly distribution does not correspond to a normal or lognormal distribution that fits either the Pearson criterion or the less rigid Kolmogorov criterion (Yaglom and Yaglom 1973). Interestingly, in the observed magnetic field distribution, the average values are close to the dispersion. This is specific to the Poisson distribution which represents the physical nature of anomalies as rare events.

The similarities in anomalies ΔT and Z_a for the Kur Depression can be explained by the northern (≈45°) dip of the disturbing bodies approximated by thin beds (Khesin et al. 1996). This assumption is corroborated by the regional geological sections through the Kur megasynclinorium. For instance, in the upper part of the sedimentary cover, there are large northern sharply dipping faults. In many cases, these faults form a plateau whose depth curls to the north. Thus, the magnetic anomaly bodies occurring in the Kur Depression section at a depth (mainly in the Ganja region) were exposed by tectonic forces oriented to the north. Hence, the

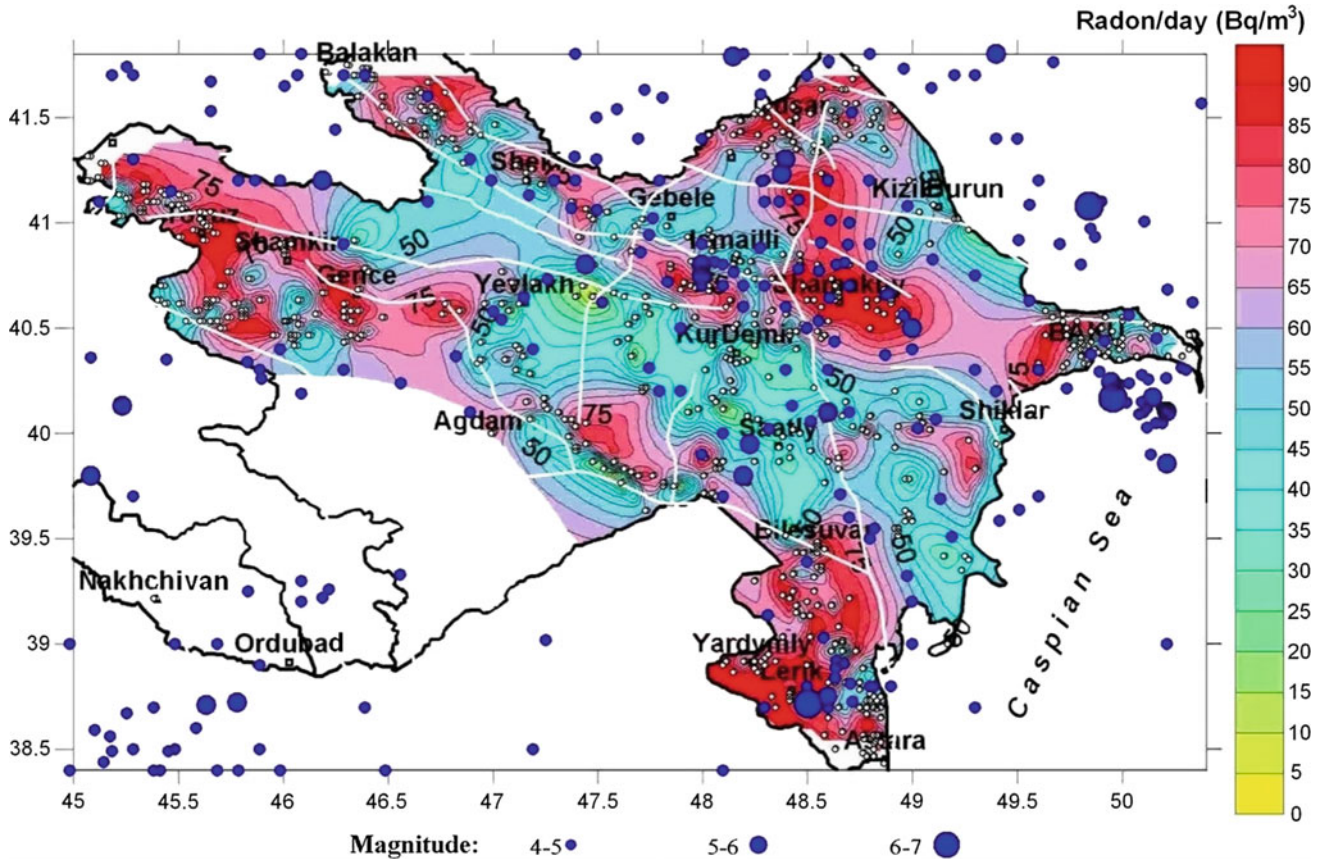

Fig. 4.9 Map of comparison of radon field of Azerbaijan with deep faults and epicenters of sensible earthquakes. *White lines* designate position of deep faults (Ch. Aliyev et al. 2012). Map of earthquake epicenters in Azerbaijan was taken from Kadirov et al. (2008)

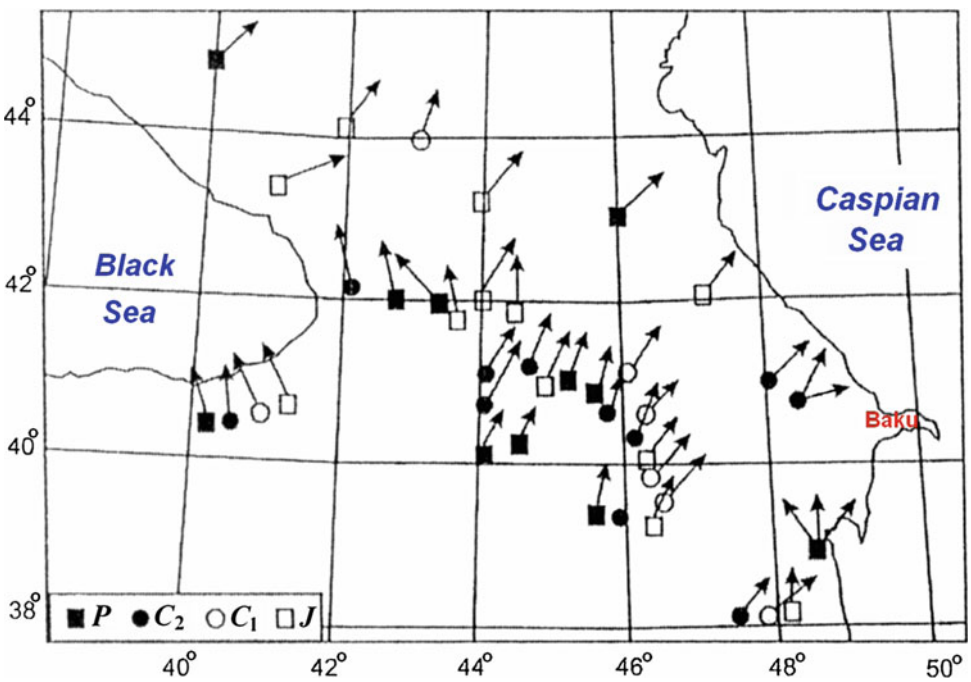

Fig. 4.10 Distribution of paleomagnetic vectors for the Mesozoic–Cenozoic rocks of Azerbaijan and adjacent areas (after Issayeva and Khalafly 2006, with some modifications). *P*—Paleogene, C_2—Late Cretaceous, C_1—Early Cretaceous, and *J*—Jurassic

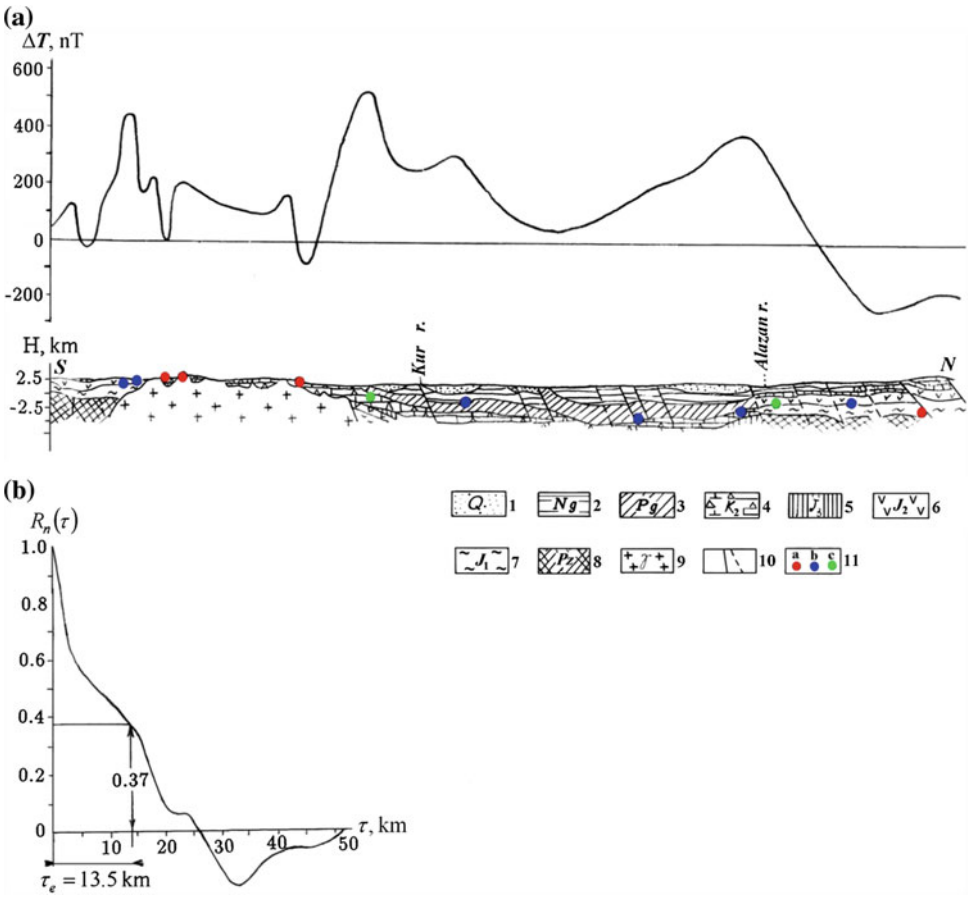

Fig. 4.11 Determination of the average occurrence depth of magnetized masses by the autocorrelation function of the magnetic field along the Gedabey-Belakan profile (Khesin et al. 1996): (**a**) ΔT plot, (**b**) the plot of the autocorrelation function. Deposits: (*1*) Quaternary, (*2*) Neogene, (*3*) Paleogene, (*4*) Upper Cretaceous, (*5*) Upper Jurassic, (*6*) Middle Jurassic, (*7*) Lower Jurassic, (*8*) Paleozoic, (*9*) intrusive rocks of the granodiorite series; (*10*) disjunctive dislocations; and (*11*) singular points of the magnetic field with the following magnetization values: **a** up to 0.5×10^{-3} CGS, **b** from 0.5 to 1×10^{-3} CGS, **c** larger than 1×10^{-3} CGS

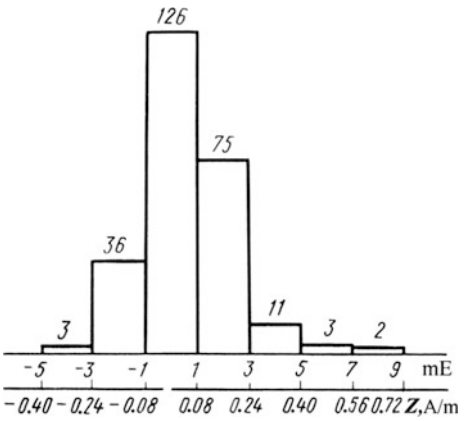

Fig. 4.12 Histogram of residual magnetic anomaly (Z component) distribution (after upward continuation to the level of 25 km) for the Lok-Garabagh zone of the Lesser Caucasus (Eppelbaum and Khesin 2012). *Values* over the histogram intervals show the frequencies of magnetic anomalies

magnetic data examination confirms the opinion of Peyve et al. (1980) and certain other investigators as to the significant role of tangential movement and the subduction of the Lesser Caucasus under the Greater Caucasus structure.

A map of predominant trends of magnetic anomaly distribution (Fig. 4.13) could be also used for regional tectonic–structural examination. Note that selected four trends (0°–45°, 45°–90°, 90°–135°, and 135°–180°) are sufficient for the description of map of any complexity.

There are several advantages of the direct use of topographic maps for geological purposes which are well known in geomorphology. Topographic data (digital terrain models) are used to determine topographic corrections in geophysics. Furthermore, the data on the terrain relief (height field) can be a source of additional geological information in processing and interpreting geophysical observations.

To summarize, the application of height field transformations enhances the informativity of a set of geophysical investigations practically without any expenditure, since the terrain height data need to be calculated for topographic effects. These transformations of the digital terrain model can be executed together with the geophysical field conversion using programs developed for computing field entropy, and curvature or the standard deviation. Obviously, the spatial distribution of the entropy values will be close to the distribution of the SSI parameter.

Various techniques of averaging are used to single out regional isometric anomalies in Azerbaijan. These include

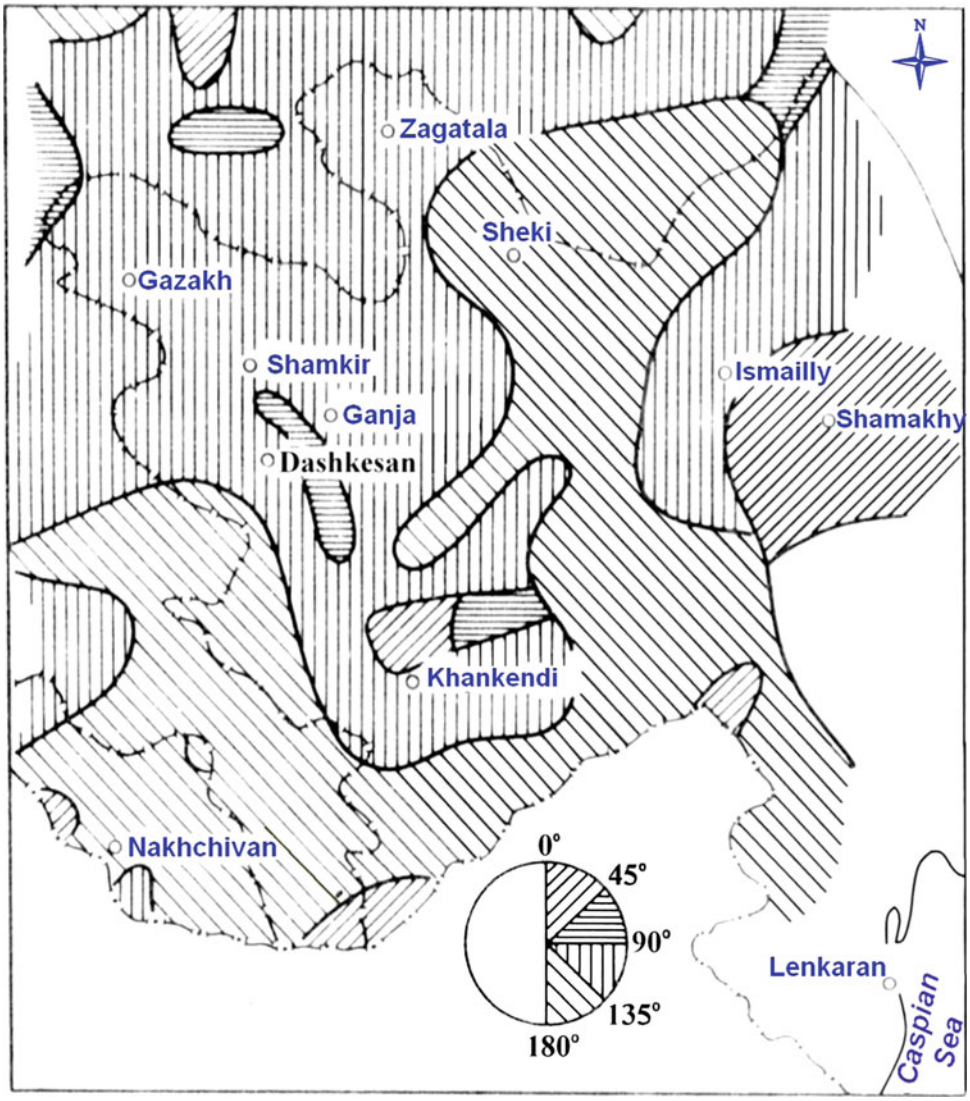

Fig. 4.13 Map of predominant trends of magnetic anomalies in Azerbaijan and adjacent regions (after Eppelbaum and Khesin 2012, with small modifications)

the method developed by Tikhonov and Bulanzhe (1945) who initiated the extensive implementation of transformations. Other techniques that are applicable are analytical upward continuation and smoothing with polynomials. However, averaging of fields with asymmetric distributions using the conventional techniques may result in distorting the regional component by the intensive local anomaly. Therefore, it is recommended to apply the method of quantiles, in particular, the median method (Borovko 1971). The 50 % quantile, the median, corresponds to the middle of the variation series composed of sequentially increasing field values within the transformation cell. To differentiate isometric anomalies by the median method, the radius r of the sliding window is chosen according to

$$r = \sqrt{r_1 r_2}, \tag{4.3}$$

where r_1 and r_2 are the radii of field features to be separated (regional and local objects, respectively) using half of their amplitude.

Usually, the transformation cell (sliding window) size should be larger than the local noise, less than the background features, and closer (or slightly higher) than the expected signal. Since there is always a correlation of results when overlapping the neighboring cells by a sliding window, it is not recommended to reduce the computation step to more than half a radius of the transformation cell.

Kunin (1968) proposed a relationship between the average area radius r and the continuation height H for the gravitational field, leading to a good fit of this transformation:

$$r \approx (2.5 \div 3)H. \tag{4.4}$$

The comparison of regional component charts of Azerbaijan obtained by averaging and upward continuation corroborates this conclusion regarding the magnetic field as well (Fig. 4.14).

Usually, the choice of transformation technique is up to the researcher. A clear physical sense of the transformation by upward continuation suggested by Andreyev and Klushin (1962), and its comparability with aircraft observations testify to the advantages of this method. However, the uncontrollable influence of the discarded residual term in Poisson's integral often turns out to be very high.

In informal calculations, along with their fundamental advantages, productivity plays an important role in the selection of the type of conversion. The median method is attractive from this standpoint. Actually, the assumption of compensation of random deviations from the average within the limits of the transformation cell (averaging method) may not hold true in smooth fields, whereas for sharply varying fields, polynomial smoothing is completely inapplicable. The results of application of the sliding average method, as shown by Borovko (1971), are more dependent on the anomaly amplitude than those of the median method. This method demonstrates very high productivity, which was confirmed by its application in Azerbaijan (Eppelbaum 2012).

High reliability can basically be attained in geophysical field regioning and reveal regional structures through areal autocorrelation analysis. However, the results of this method are highly dependent on the field description interval and the size of a sliding window. In addition, this analysis is accompanied by a significant loss of the area on the map edges and only yields general results, which rarely or never have individual value.

4.2.2 Gravity Data Analysis

The difference field ("ring" anomalies) $\Delta g_{B(8-20)}$ which is present to a significant extent in the mountain-folded regions reflects the influence of the internal structure and inhomogeneities of the consistency of the metamorphic basement (Baikalian folded basement) and deeply occurring (and buried) parts of intrusions in the Kur Depression, in general the influence of Mesozoic associations (Khesin et al. 1996). This map is shown in Fig. 4.15.

An informational parameter can be effectively applied for the regional gravity field processing (Eppelbaum 2014). It is well known that the South Caspian basin (*SCB*) is one of the main hydrocarbon provinces in the world (Mamedov et al. 2008). The satellite gravity data of the *SCB* were obtained from the World Gravity DB as retracked from Geosat and ERS-1 altimetry (e.g., Sandwell and Smith 2009). A highly positive factor is that these observations were made with regular global 1-min grids, and the error of gravity data computation for the newly arrived data is estimated at 1.0–1.5 mGals (Sandwell et al. 2013). The gravity data retracked to the Earth's surface are close to free-air gravity and can be effectively applied to the tectonogeophysical zonation (Eppelbaum and Katz 2011). The compiled gravity map (Fig. 4.16a) shows the gravity pattern within the *SCB* and southwest land bordering. The gravity data are ranging from −180 up to +420 mGals, and the anomalies in the center of the *SCB* are not brightly expressed. After application of the informational approach (Eppelbaum 2014), the image was significantly transformed (Fig. 4.16b) and the gravity anomalies in the *SCB* can be effectively recognized (it should be noted that in the both maps, the same color pattern was applied).

Such a satellite imaging of various geophysical fields (gravity, magnetic, infared, etc.,) in different scales is a powerful interpretation tool of the nearest future.

One of the most effective gravity field transformations in Azerbaijan was demonstrated in Kadirov (2000b). Gravity data acquired in the Shamakhy-Gobustan and Absheron oil- and gas-bearing regions (Fig. 4.17) were filtered using a Hartley transform (HT) and Butterworth filter (BF).

Figure 4.18 shows the Bouguer gravity map of the study area. The gridded square constructed on the basis of the Bouguer gravity data set has 32 × 32 elements both in the west-to-east and south-to-north directions, with the grid interval taken every 5 km in both directions.

The Eastern Azerbaijan negative anomaly with an extreme value at −140 mGal covers the Absheron-Gobustan area; this type of anomaly is not the characteristic of areas of high topography. The Dubrar relative maximum, stretched along the southeast slope of the Greater Caucasus, is located in the northwest part of the area. Another non-extensive relative maximum zone goes in the direction from the Yavany Mt. to the Sangachal locality. The axis of this anomaly is stretched parallel to the direction of the Greater Caucasus axis. Some of the local anomalies are overshadowed by the regional anomalies clearly outlined in the map.

The 2D HT of a real function $f(x, y)$ is defined (after Hartley 1942) as:

$$H(u,v) = \int_{-\infty}^{\infty} \int_{-\infty}^{\infty} f(x,y)\mathrm{Cas}(ux) \cdot \mathrm{Cas}(vy)\mathrm{d}x\mathrm{d}y, \quad (4.5)$$

where $\mathrm{Cas}(ux) \cdot \mathrm{Cas}(vy) = \cos(ux - vy) + \sin(ux + vy)$.

The ideal low-pass BF is given by (Kulhanek 1976):

$$H_B(k) = \frac{1}{\sqrt{1 + \left(\frac{k}{k^c}\right)^{2n}}}, \quad (4.6)$$

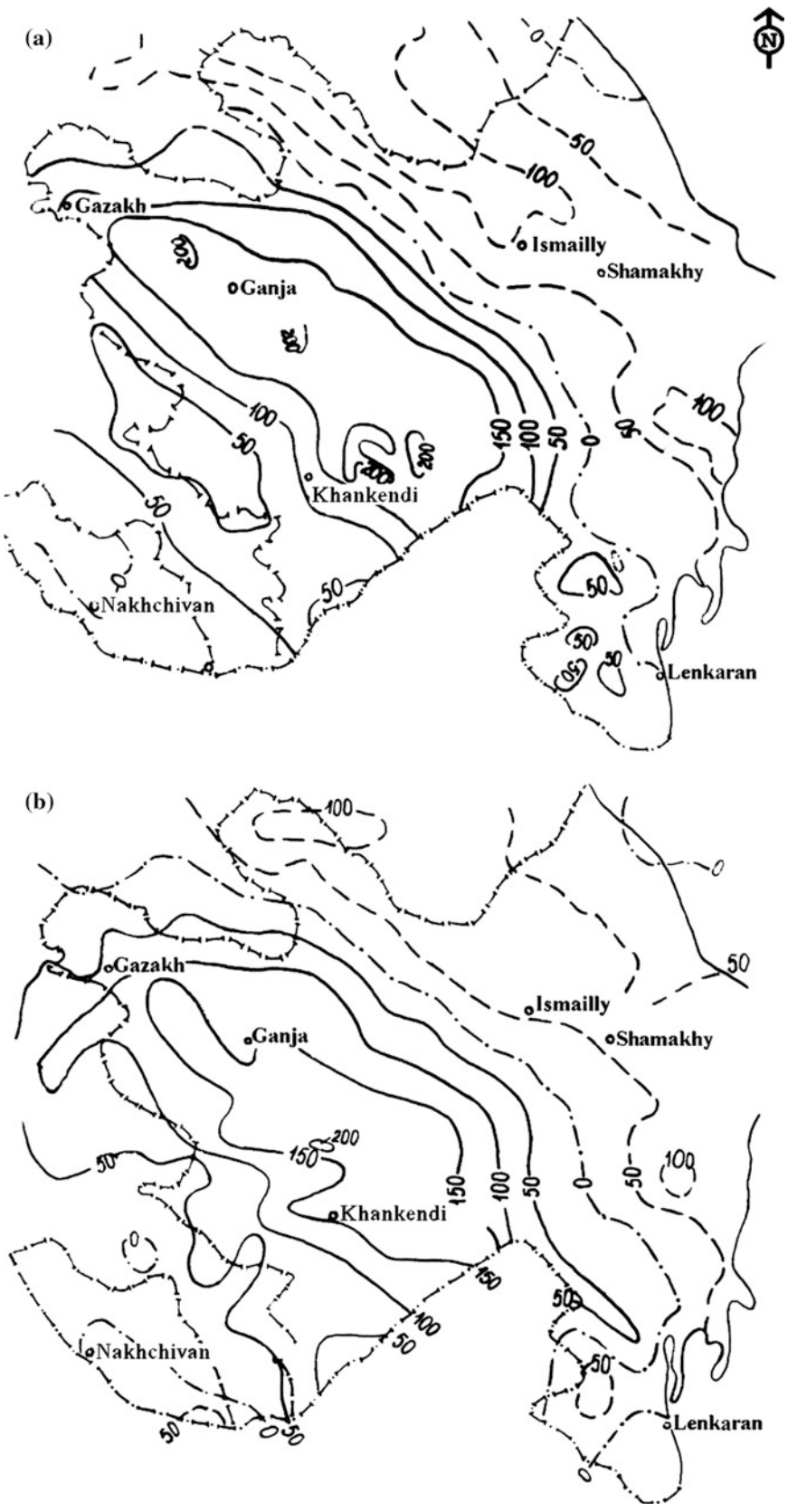

Fig. 4.14 Singling out the regional component of the magnetic field in Azerbaijan: (after Eppelbaum and Khesin 2012). **a** average within a radius of 60 km; **b** continued upward to a height of 25 km. Isolines in nanoTesla: (*1*) zero, (*2*) positive, (*3*) negative

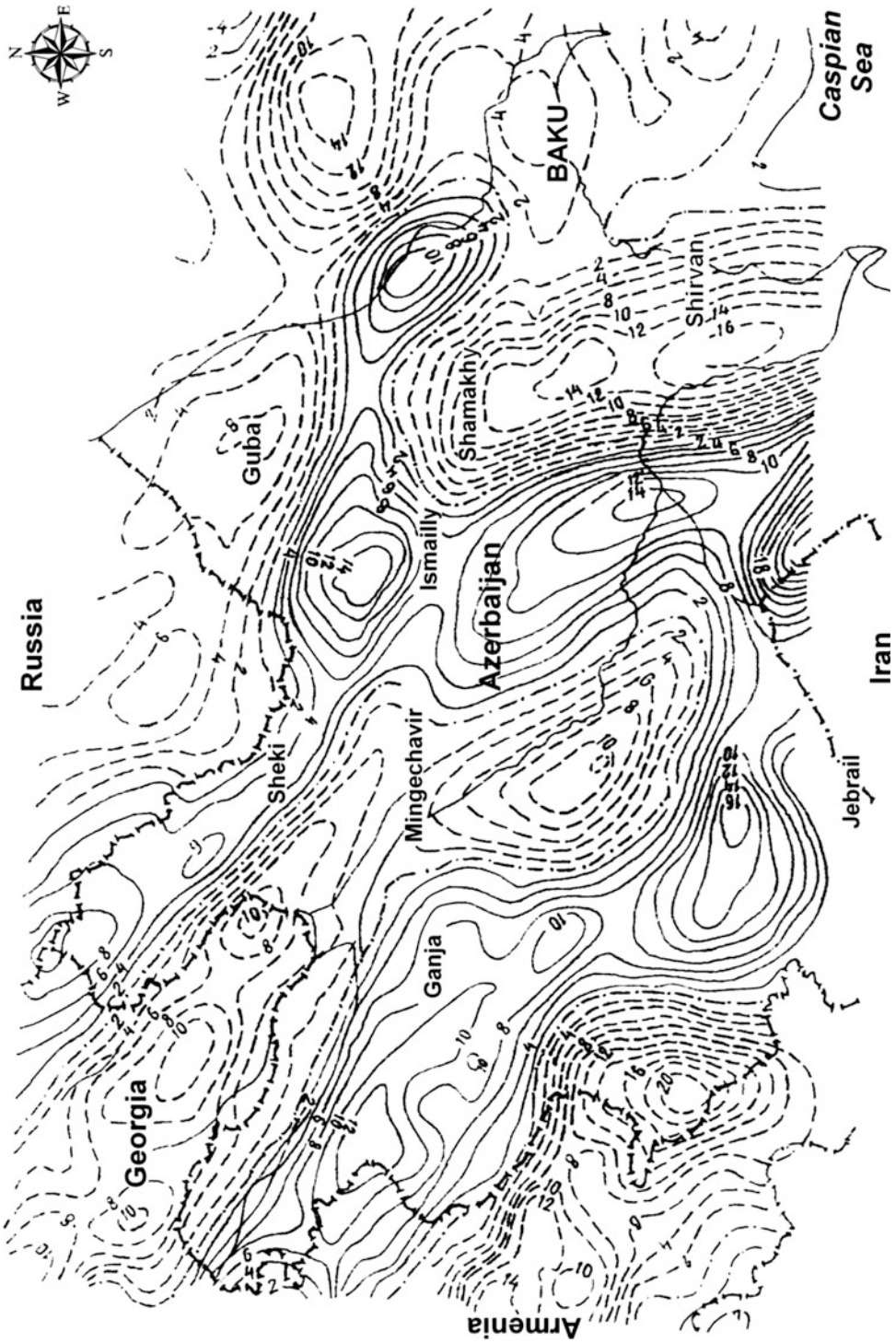

Fig. 4.15 Map of difference Δg_{8-20} anomalies computed as the difference between upward continued fields in the Bouguer reduction (terrain correction was computed with a radius of 200 km and the density of the intermediate layer was defined as 2.67 g/cm^3) at heights of 8 and 20 km, respectively (Khesin et al. 1996; Kadirov 2000a; Gasanov 2001)

where $k = \frac{2\pi}{\lambda}$ is the wave number, $k_c = \frac{2\pi}{\lambda^c}$ is the cutoff wave number, and n is the degree of the filter. In this study, n was taken to be equal to 1. The procedure of filtering is using the HT transform, the gridded gravity data are converted to space–frequency Hartley domain. In this domain, row by row followed by column by column Butterworth filters are applied using a suitable cutoff frequency. Then, the produced filters are multiplied by the spectrum of data in the Hartley domain. Finally, by taking the inverse transform, the mathematical processing was returned to the space domain (Kadirov 2000b).

The calculated power spectrum curve (by the use of Fourier transform (FT)) is displayed in Fig. 4.19. The power spectrum of the gravity data shows a cutoff wave number

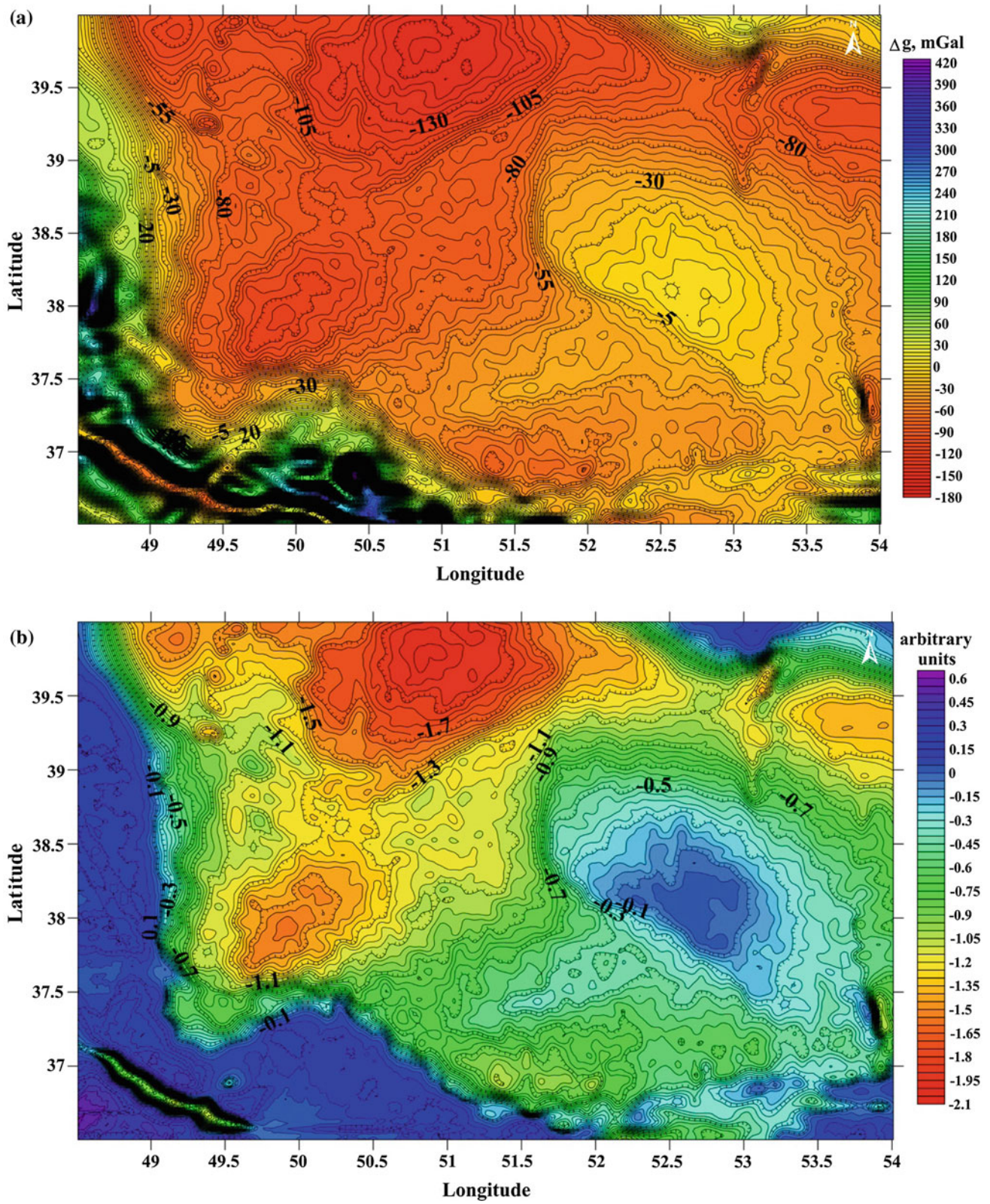

Fig. 4.16 **a** Satellite gravity map of the South Caspian basin and its SW border compiled on the basis of Geosat and ERS-1 altimetry data (Eppelbaum 2014). **b** Map of the informational parameter I_i transformed from the map shown in Fig. 4.16a (Eppelbaum 2014)

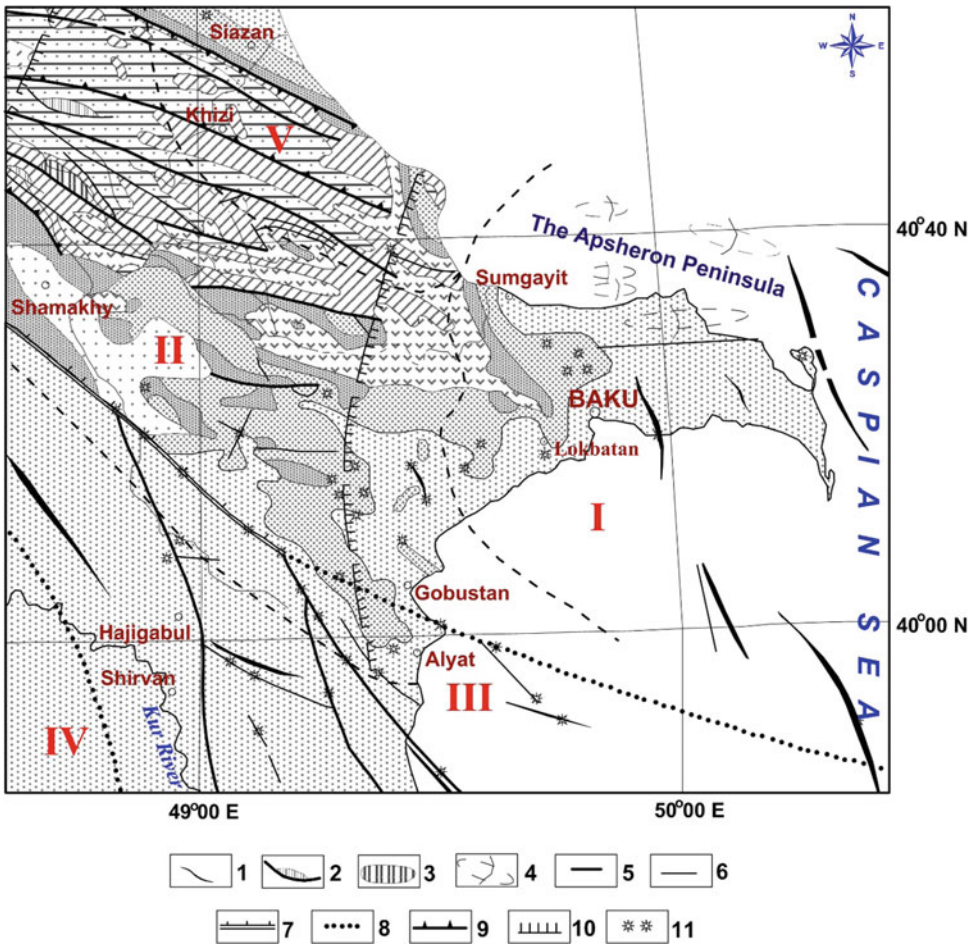

Fig. 4.17 Tectonic–geological scheme of the study area. Alpine orogenesis subcomplexes: (*1*) early orogenesis subepoch ($O_1^1 AP_3 - N_1$), (*2*) early orogenesis upper epoch ($O_1^2 A N_1^2 - N_1^2$), (*3*) late orogenic epoch up to 800 m ($O_2 A N_2^3 \ N_2^3 - Q$), and (*4*) late orogenic epoch 800 m and greater (O_2). Structural elements, fold types, and dislocations with a break in continuity: (*5*) axes of large anticlinal folds, (*6*) scale-shaped folds, (*7*) tectonic nappe, (*8*) buried folds, (*9*) normal faults with thousands of meters of amplitude, (*10*) normal faults with hundreds of meters of amplitude, (*11*) crustal faults manifested at the surface by thrusts and overfaults, (*12*) buried faults, (*13*) thrusts and overfaults with thousands of meters of amplitude, (*14*) buried flexure, (*15*) mud volcano. Oil- and gas-bearing regions: *I*—Absheron region, *II*—Shamakhy-Gobustan region, *III*—Baku archipelago, *IV*—Lower Kur region, *V*—near-Caspian region (after Kadirov 2000b, with modifications)

separating two domains of high- and low-wavelength information. The low- and high-wave number parts of the power spectrum, associated with deep and shallow gravity sources, were taken as representing the regional and residual anomalies, respectively. Two linear segments shown in the plot are suggestive of the existence of discrete density boundaries, with the slopes being the estimates of their mean depths (Bhattacharyya 1966; Spector and Grant 1970). The present power spectrum indicates a depth of 24.5 km for the long-wavelength component and a depth of 3.2 km for the short-wavelength component. These depth values are well-correlated with the results of seismic studies previously carried out in the region.

The cutoff wave number is determined by the crossing point of fitted straight lines approximating the power spectrum data in the high- and low-wavelength domains. A cutoff wave number of k_c is found from the c power spectrum.

Figure 4.20 shows the results of low-pass filtering arranged for a k_c 0.142 km^{-1} wave number. The gravity minimum north of Absheron is reflected in the regional Bouguer anomaly map. The results of the high-pass filtering process are shown in Fig. 4.21. A large positive anomaly is evident northwest of the region from Sumgayit to Siazan, the so-called Dubrar positive anomaly. A maximum local anomaly value of 7 mGal is noted in the Khizi locality. Another extensive positive anomaly lies parallel to the Greater Caucasus axis covering an area from the Yavany Mt. to Sangachal, where the highest value is equal to 3 mGal. In the southwest, a large positive anomaly located within the

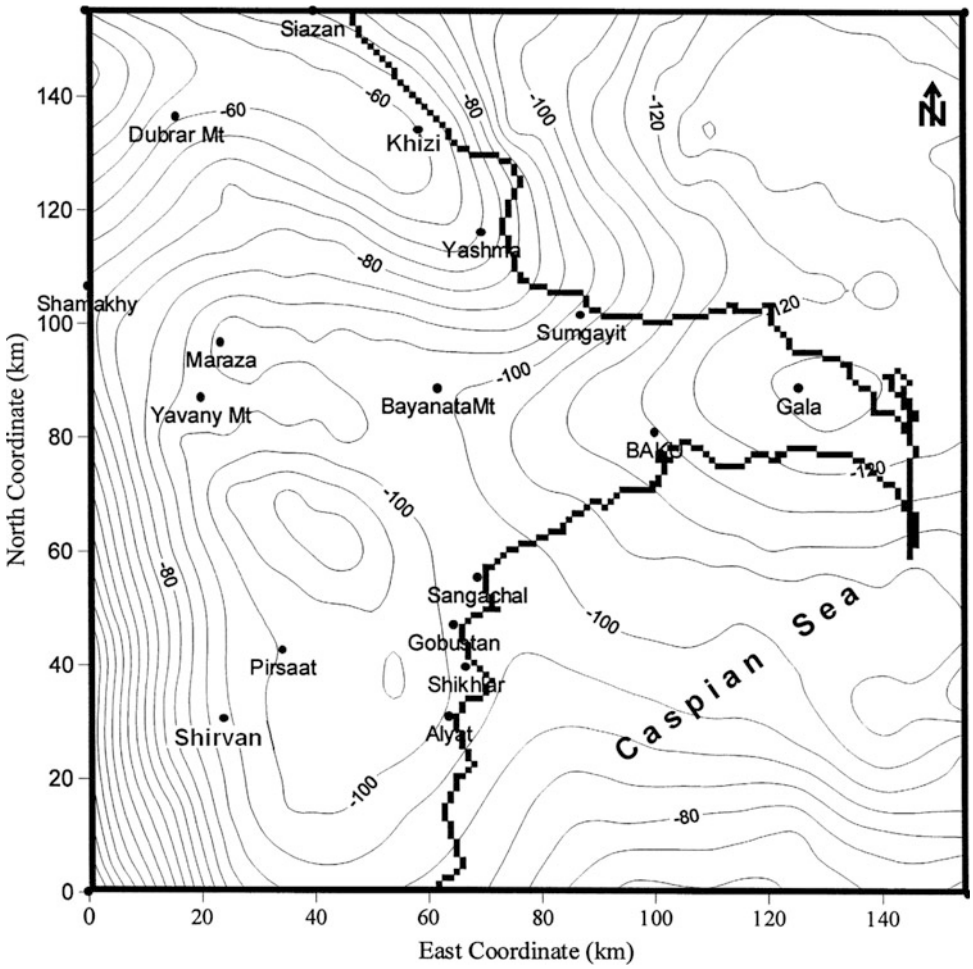

Fig. 4.18 Bouguer gravity map for the study area. Contour interval is 5 mGal (Kadirov 2000a)

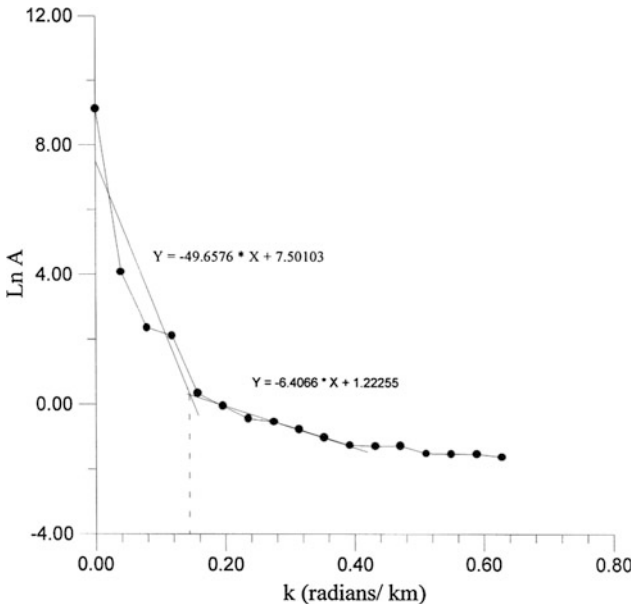

Fig. 4.19 Power spectrum of the Bouguer gravity anomaly in the study area (Kadirov 2000b)

Kur Depression is noted. The Absheron-Central Gobustan negative anomaly (as low as −7 mGal) is seen to the east and south of the Dubrar Mt. positive-anomaly region. The Absheron negative anomaly extends toward the north. A row of closed negative anomalies begins from Gobustan and goes toward Shamakhy. The results of the high-pass filtering through the FT are shown in Fig. 4.22. As can be seen, the contours shown in Figs. 4.21 and 4.22 are very similar ones.s

The depth occurrence of the pre-Mesozoic crystalline basement surface has been studied with the aim of interpreting the gravity anomalies in the Absheron and the Shamakhy-Gobustan regions. The density versus depth relationship in the part of the Earth's crust overlying the crystalline basement can be approximated by a quadratic function (Bhaskara Rao 1986). The computed function for the area under study is shown in Fig. 4.23.

The depth map of the basement in Fig. 4.24 is estimated from the inversion of the "residual" gravity field constrained with the density model (Fig. 4.23) by using the GR3DSTR program (Bhaskara and Ramesh 1991).

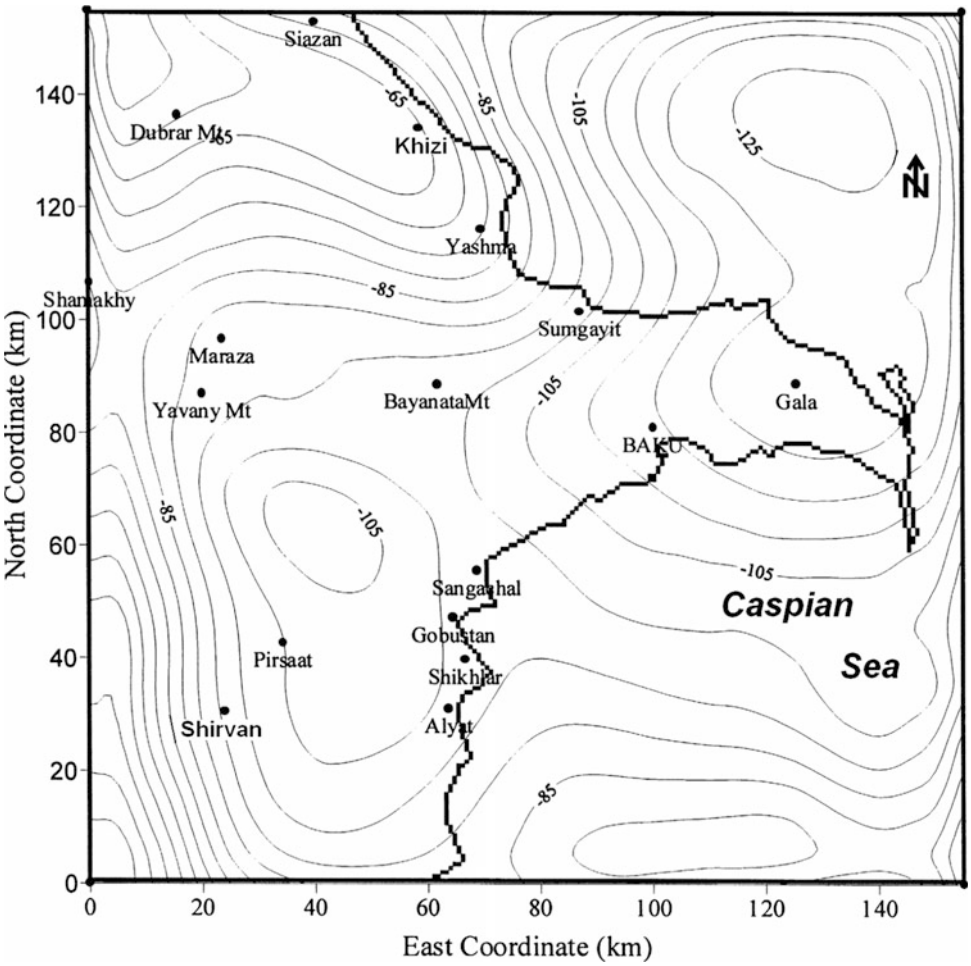

Fig. 4.20 Results of the low-pass filtering of the gravity data on the study area using 2D HT (Kadirov 2000b)

Calculations for the basement depth maps were performed at specified 10 iterations. The recalculated gravity effect based on the depth-to-basement map (Fig. 4.24) is shown in Fig. 4.25. Apart from the regional shift of 30 mGal, the map agrees well with the regional-anomaly map. As can be seen, higher values on the map correspond to the Yavany Mt.—Alyat area where the mean depth is around 23 km. The mean depths in the Absheron Peninsula and the Dubrar zone are 20 and 6 km, respectively. The data presented are well-correlated with the results of seismic exploration (e.g., Aksyonovich et al. 1962; Gadjiyev 1965; Radjabov 1978).

Regional gravity anomalies in the Caucasus-Caspian region were successfully studied in Kadirov (2004).

Upward continuation of gravity data is widely used in geophysics. It can be used, for example, to enhance the signal of deeper sources when shallower ones are present. Mantle anomalies of the gravity field ("geodynamic reduction") obtained through the elimination of impact of the upper layers is determined by analytical continuation into the upper half-space—to the altitude of more than 50 km (Kaban 2000; Kadirov 2000a, b). Values of depth of occurrence of abnormal bodies calculated with logarithm of the power spectrum determined by analytical continuation of regional gravity field allow to make a conclusion about the necessity of application of these anomalies as reflectors of mantle gravitation effect (Kadirov 2000a). Gravitation model of the region may be considered as one of the main factors of geodynamic constructions.

Kadirov (2004) applied the Hartley transform (Hartley 1942) for upward continuation of the gravity data on the Caucasus-Caspian regions, recalculation of gravity anomalies for different heights, and computation of horizontal gradient of gravity field for unmasking some regional tectonic–structural peculiarities.

Gravity field in the studied area in the Bouguer reduction (Fig. 4.26) includes the territory of the Middle and the South Caspian and territories of Azerbaijan, Georgia, Armenia, south of Russia, west of Turkmenistan and Kazakhstan as well as eastern Anatolian and northern Iran. The gravity map in the Bouguer reduction is constructed with the value of the interstitial layer density of 2.67 g/cm^3. Normal value of the gravity was calculated by the Helmert Eq. 1909 with account of amendment—14 mGal. While calculating the Bouguer anomalies, relief of the locality was taken into

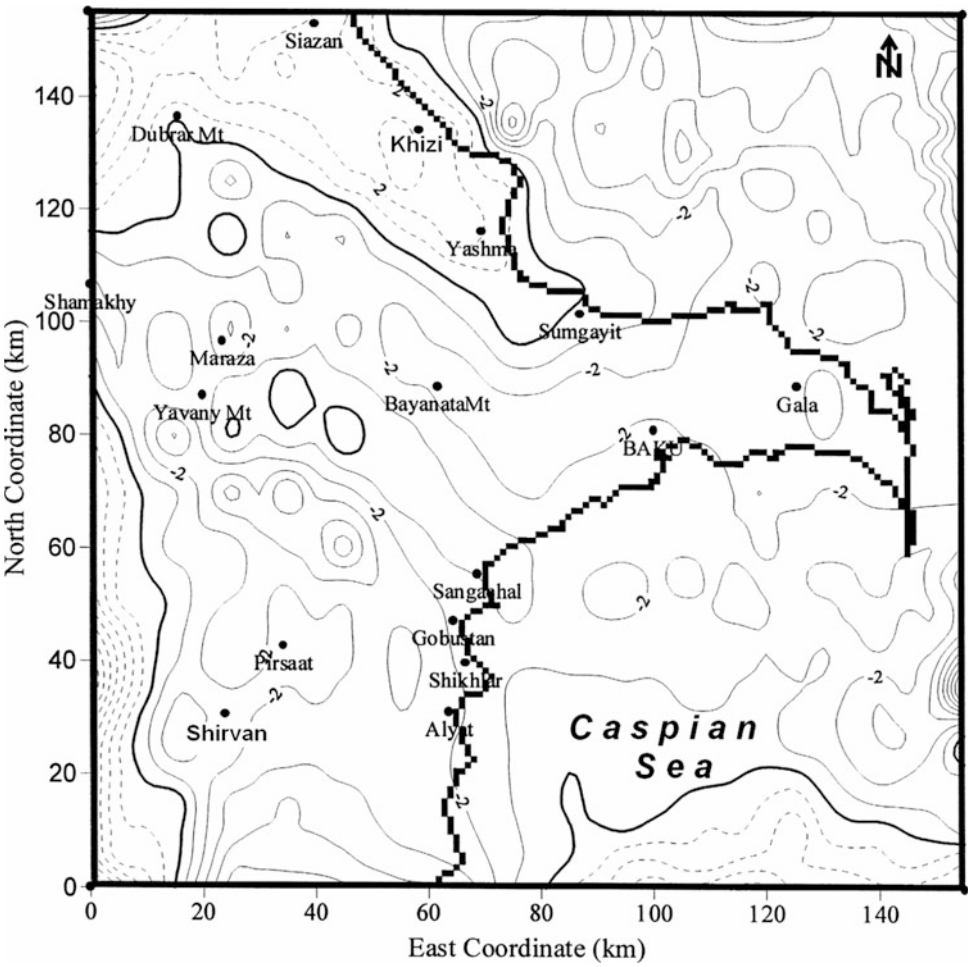

Fig. 4.21 Results of the high-pass filtering of the gravity data on the study area using 2D HT. *Dashed* and *solid lines* show positive and negative local anomalies, respectively (Kadirov 2000b)

account (R = 200 km). For the offshore areas, the gravity map is constructed with account of amendments for the surrounding relief and for the seafloor topography (Gravity map of the USSR 1990). In the summary map of the Bouguer anomalies in the investigated region, one can identify a pan-Caucasian background of negative anomalies. A vast positive regional anomaly occupies a part of the Middle Caspian and a part of territories of Turkmenistan and Kazakhstan (Aktau-Bekdash-Turkmenbashy). This maximum is adjacent to Dagestan, East Azerbaijan, and Tcheleken minimums linked with each other by a narrow line. From the west, the East Azerbaijan minimum is limited by the Azerbaijan maximum. The latter with values of the gravity varying from 0 to 100 mGal is mainly associated with the Lower Kur Depression and partially spreads over the Talysh Mts. This maximum has two "fingers" in the form of narrower relative maximums (anomalies from 0 to 50 mGal). One of them stretches northward and connects with the Alazan zone. Another one goes northwestwards through the city of Ganja as far as Tbilisi and spreads over a narrow line of uplifts along the northwest margin of the Lesser Caucasus.

Regional anomalies of the gravity field in the Caucasus-Caspian region are investigated by recalculation of data of the gravity field for different altitudes. In the zone of frequency, the gravity field at a height of z is calculated by the product of 2D spectra of the input function and weight function:

$$F_u(u, v, -z) = A(u, v) \exp\left(-z\sqrt{u^2 + v^2}\right), \quad z > 0, \quad (4.7)$$

where $F_u(u, v, -z)$ is the result of analytical continuation to the height in the frequency zone, $A(a, v)$ is the spectrum of the input function, and u and v are the spatial frequencies in x and y directions, respectively (Blakely 1995).

The spectrum of the input function is calculated with the application of Hartley transform (Hartley 1942; Sundararajan 1995; Kadirov 2000a). And further with the help of reverse Hartley transform, we return to the spatial zone. Recalculation of gravity anomalies was carried out for altitudes 20, 50, and 100 km. In compliance with geologic–geophysical investigation, one may suppose that the first altitude corresponds approximately to the average depth of the surface of a "basaltic" layer. The second altitude

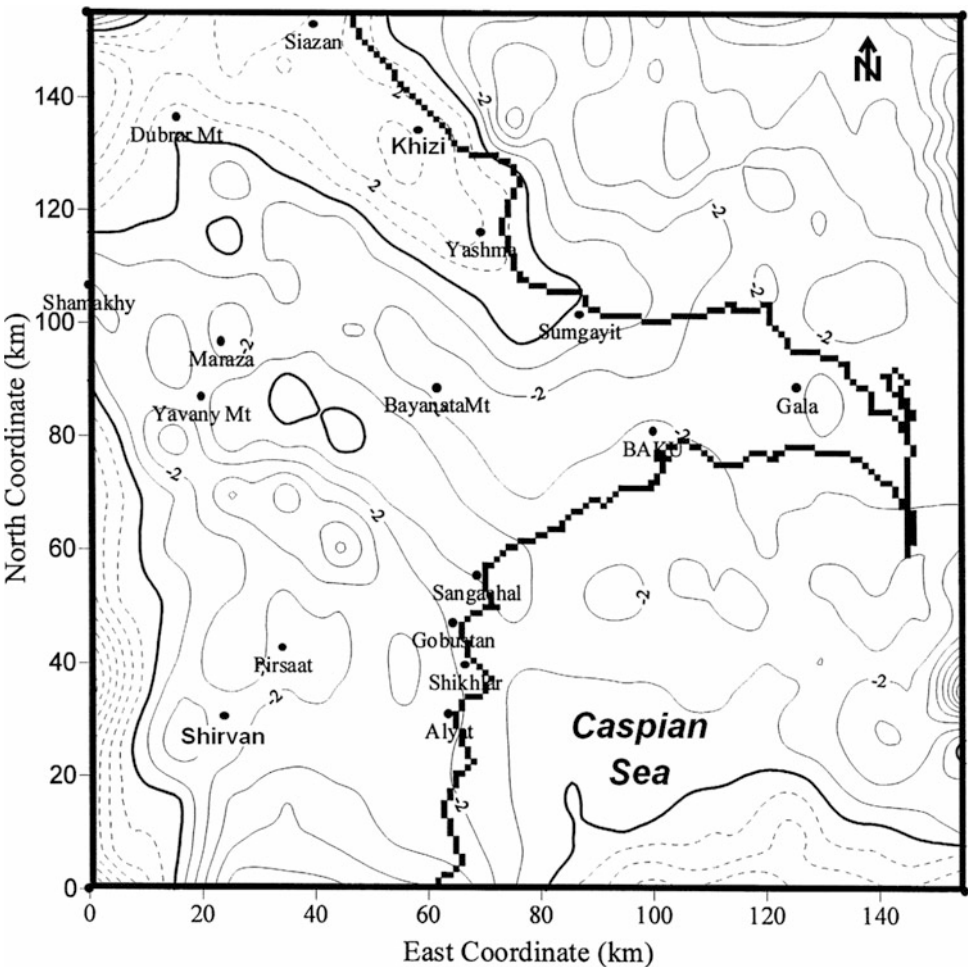

Fig. 4.22 Results of the high-pass filtering of the gravity data on the study area using 2D FT. Dashed and solid lines show positive and negative local anomalies, respectively (Kadirov 2000b)

corresponds to the depth of Moho discontinuity occurrence. Other altitude corresponds to depth in the upper mantle. For this reason, they are taken by us for "geodynamic reduction." Figure 4.27 demonstrates gravity anomalies of the region recalculated for the altitude of 20 km. Negative and positive anomalies are marked by continuous and dotted lines. The southeast of the Caspian Sea, Kara-Bogaz bay, and Aktau and Bekdash districts are overlapped by a positive anomaly (+40 mGal). The central part of this isometric anomaly is situated in Bekdash where values of amplitude are up to 60 mGal. Other positive anomalies are observed in Talysh (20 mGal), Safidrud (5 mGal), and 30 km to the west of Okerem (5 mGal).

Figure 4.28 shows the distribution of the gravity field in the Caucasus-Caspian region recalculated for the height of 50 km. The isoline contour interval is 5 mGal. Preservation of the north Absheron minimum recalculated for the height of 100 km in the maps of gravity anomalies demonstrates that this regional minimum is linked partially with density boundaries located below the Moho discontinuity (Kadirov 2000a). Comparison of gravity anomalies determined by possible density boundaries in the upper mantle with results of the investigation by other methods of the mantle structure is of a certain interest.

One can see that the Bekdash positive anomaly is preserved with the amplitude of 25 mGal. Relative maximum manifests itself in Talysh and in the south of the Caspian Sea. In the Lesser Caucasus and in the Absheron Peninsula, one can observe gravity minimums. Most of the regional anomalies are linked with the change of depth of the Moho discontinuity occurrence.

Distribution of gravity anomalies at the altitude of 100 km is shown in Fig. 4.29. At the altitude of 100 km, minimum of the gravity field is −105 mGal and maximum is +8 mGal. Gravity anomalies of the region recalculated to the height of 100 km indicate that the gravity field became much simpler and is displaced in the south direction of the center of the above-mentioned large negative anomalies. Regional anomalies for these cases are linked with the depth of occurrence of the layer surface in the upper mantle. Isolines of the regional anomaly in the Lesser Caucasus are bended in Khankendi in the northeast direction. In the Absheron Peninsula, negative anomaly is preserved. Maximums of the gravity field in Talysh and Safidrud and the southeast

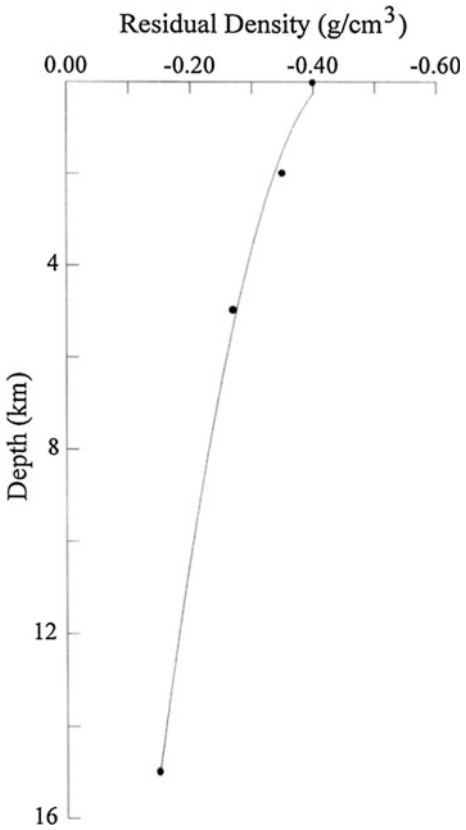

Fig. 4.23 Approximation of density versus depth data for the study area by a quadratic function

Caspian are united into one relatively positive anomaly. The anomaly in the Absheron Peninsula preserves its Caucasian orientation.

On the base of analysis of data of the gravity field recalculated for the height of 100 km as well as anomaly of velocity of the propagation of seismic waves in the asthenosphere, heat field in the surface of the mantle under the eastern part of the Absheron Peninsula, one should anticipate intensive disconsolidation of the matter in the asthenosphere (Vinnik 1976; Shengelaya 1984; Kadirov 2000a). In other words, these results allow to suppose that regional anomalies of the gravity field (recalculated for the height of 100 km and corresponding to the depth of asthenosphere) in the Absheron Peninsula are determined by the properties of the upper mantle.

Deep subvertical boundaries in the territory of Azerbaijan and adjacent regions were detected by computing gravity field horizontal gradient in different modifications (Kadirov 1998, 2004).

Value of a total horizontal gradient of the gravity field in Azerbaijan varies between 0 and 5.63 mGal/km. Maximum calculated values of the horizontal gradients for Azerbaijan are >1.5 mGal/km (Kadirov 2000a). Figure 4.30 demonstrates shaded relief map of total horizontal gradients of the gravity field in the Caucasus-Caspian region. Field of the gradients is a rather complex picture. One can clearly see superposition of gradient zones of different intensity and width. To identify interblock boundaries, there were determined horizontal gradients of gravity anomalies which are maximums. The identified values are united nearly everywhere into extended zones corresponding to the boundaries of the blocks. In the shaded relief map of total horizontal gradients of the gravity field, one can clearly see the plan of location of subvertical contacts of rocks of a different abnormal density.

Figure 4.31 demonstrates a map of total horizontal gradients of a regional field, recalculated for the altitude of 20 km and its shaded relief map. In the shaded relief map of the horizontal gradients of the regional field, there were shown lines corresponding to vertical boundaries. Figure 4.32 demonstrates that the pre-Caucasian (Makhachkala-Turkmenbashy), Siazan, major-Caucasian, pre-Lesser Caucasian (Kur Depression), Lagich-Kyzylagach, Dilidjan-Lachin-Ardabil, and north Ajinohur faults find their reflexing in the regional anomaly of the gravity field, recalculated for the altitude of 20 km (Gadjiyev 1965; Borisov 1967; Shikhalibeyli 1996). The zone of the crushing by these faults may be related to the depth of occurrence of the "basaltic" layer. A number of longitudinal and cross-linear elements in the distribution of maximums of the horizontal gradient of the gravity field manifest themselves as well. A linear trend in the distribution of maximums of horizontal gradients of the gravity field—the Agdash linear element stretching from the north to the south as far as 150 km—is of a certain interest. In the north deep, faults cut into this linear element in the south slope of the Greater Caucasus.

4.2.3 Thermal Data Analysis

Computation of vertical and horizontal gradients of temperature field is widely applied tool for revealing some desired geological–geophysical peculiarities (e.g., Somerton 1992; Beardsmore and Gull 2001; Eppelbaum et al. 2014).

When defining temperature at intersection points of rectangular grid, horizontal gradients are calculated using finite difference method. Map of distribution of total horizontal geothermal gradients at 5000 m depth is shown in Fig. 4.33. It may be seen from this map that the maximal values of total horizontal gradients correspond to active regional fault zones (Mukhtarov 2012). Besides this, some examples of thermal data analysis are also shown in Chap. 5 of this volume.

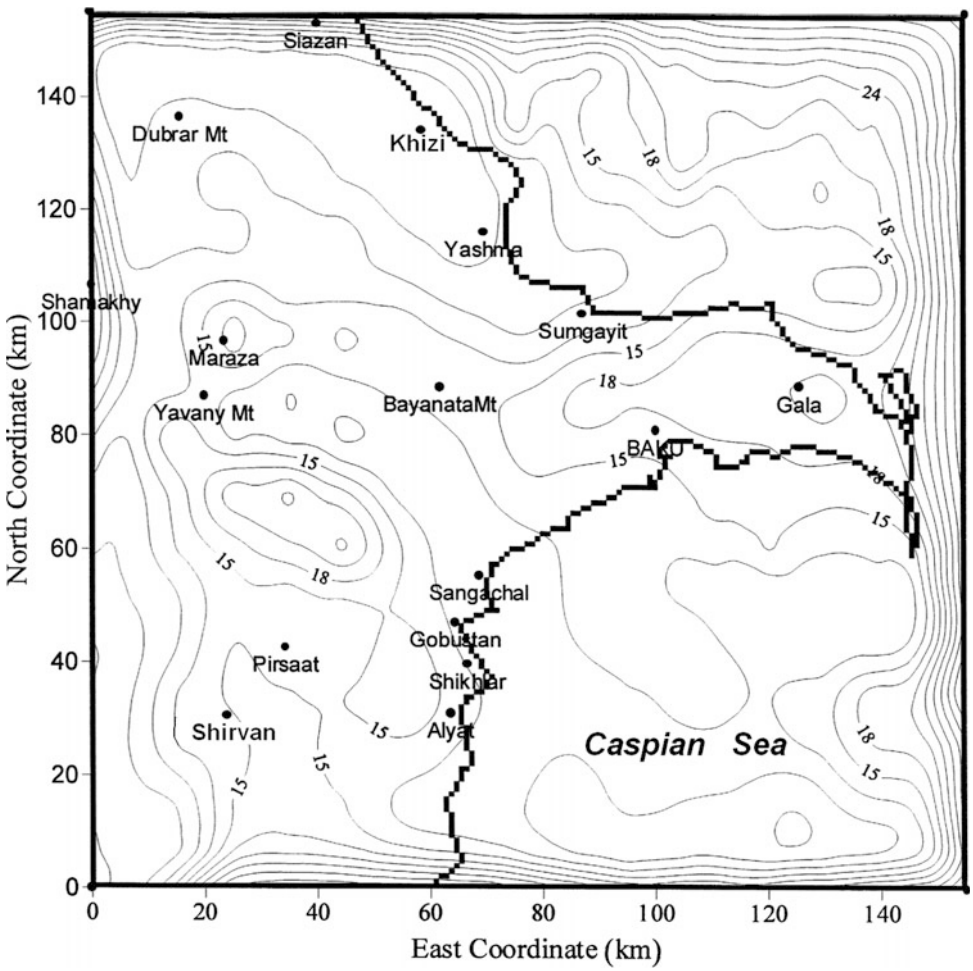

Fig. 4.24 Basement contour map of the study area derived from 3D modeling of gravity anomalies using a quadratic density function. Contour interval is 3 km (Kadirov 2000b)

4.2.4 Topography Data Analysis

Geological regularities, which manifest themselves in mountainous relief structures, can be highlighted by treating the height field of the area with the techniques employed in geophysical field analysis. For example, Borovko (1971) presented an effective application for anomalous object by the predominant strikes of relief isohypses. Later (Khesin et al. 1996) showed that this transformation can identify a very important indicator of endogenic deposits of various compositions and origins (Fig. 4.34). Large deposits tend to occur in the corners of blocks having a predominant strike of isohypses that differs from the Caucasus as the whole. This led to the recommendation to drill deep test wells in the mountainous regions of Azerbaijan.

The relief complexity, which was described above, governs the spatial distribution of topographic corrections and can be estimated by a map of the specific sinuosity of height isolines. Khesin et al. (1983) proposed applying the specific sinuosity of isolines (*SSI*) to characterize the complexity of a geophysical field.

It is calculated as follows: (1) the total length of isolines (L) for a given field is computed within a sliding area, (2) area S on the sliding cell is calculated, and (3) the parameter

$$SSI = KL/S, \tag{4.8}$$

is computed, where K is the scale factor for converting L into kilometers and S into square kilometers. The *SSI* parameter is measured in km/km^2, and the value obtained refers to the center of this cell.

In order to identify the general features of geophysical fields (and the height field as well), it is often advisable to calculate tertiary indicators, i.e., SSI by formula (4.8), the length of dislocations obtained by sliding window calculations (Khesin et al. 1996).

The SSI distribution (Fig. 4.35) reflects certain geological features of the region. Interestingly, this chart correlates rather well with the map of seismic activity (Riznichenko et al. 1983).

The role and significance of various indicators in the indicator space is different when the goal is regioning. Here,

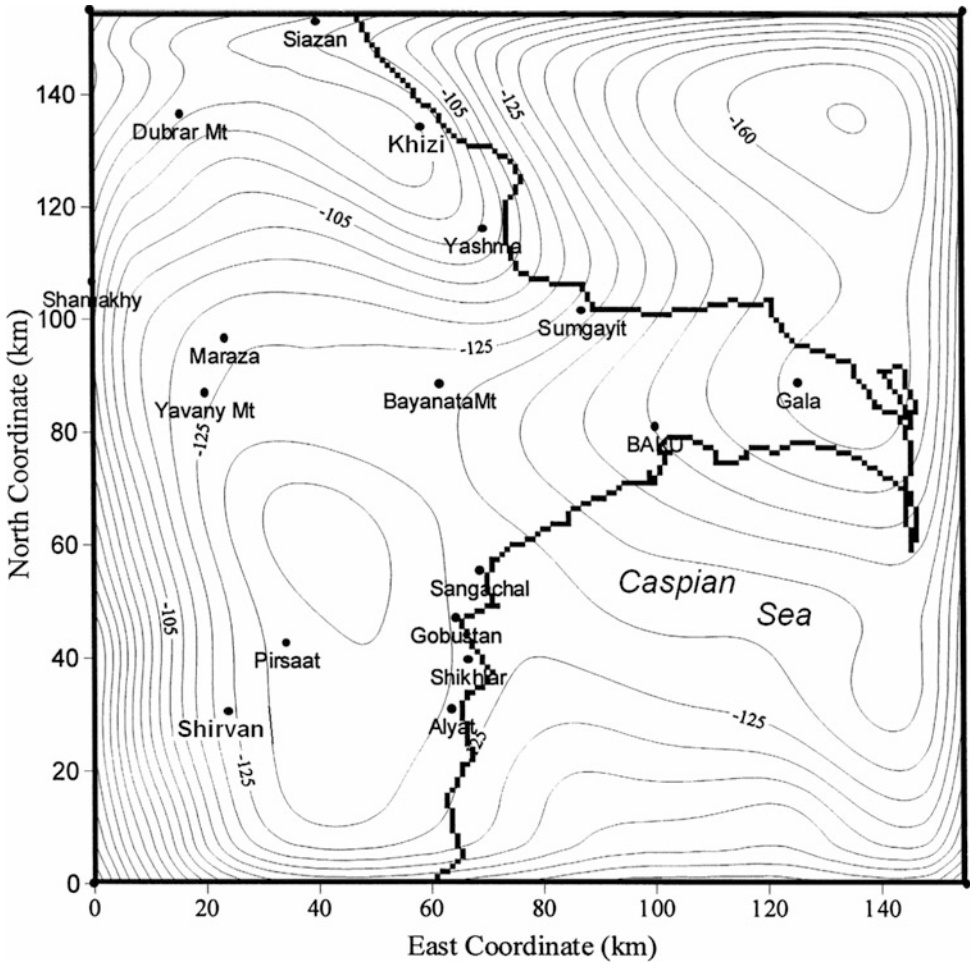

Fig. 4.25 The calculated gravity anomalies of the sedimentary basin with the 3D prism program. Contour interval is 5 mGal (Kadirov 2000b)

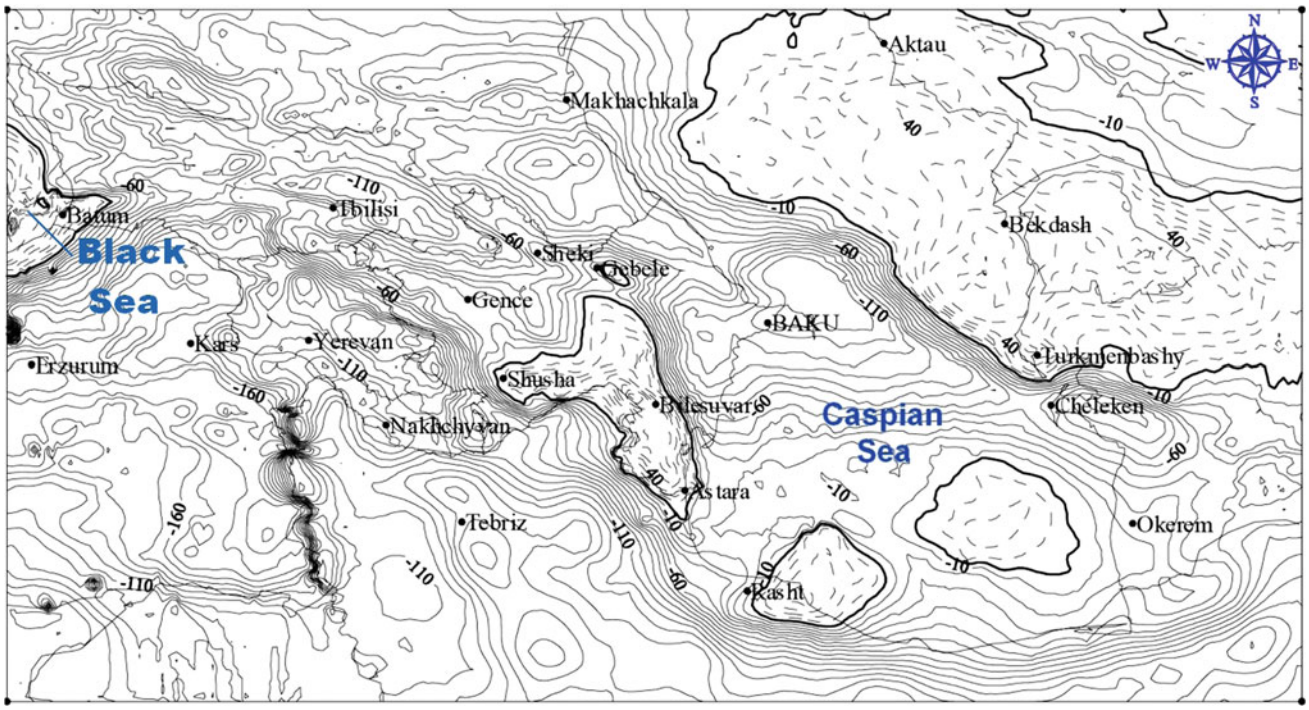

Fig. 4.26 Bouguer gravity map of the Caucasian-Caspian region (Kadirov 2004)

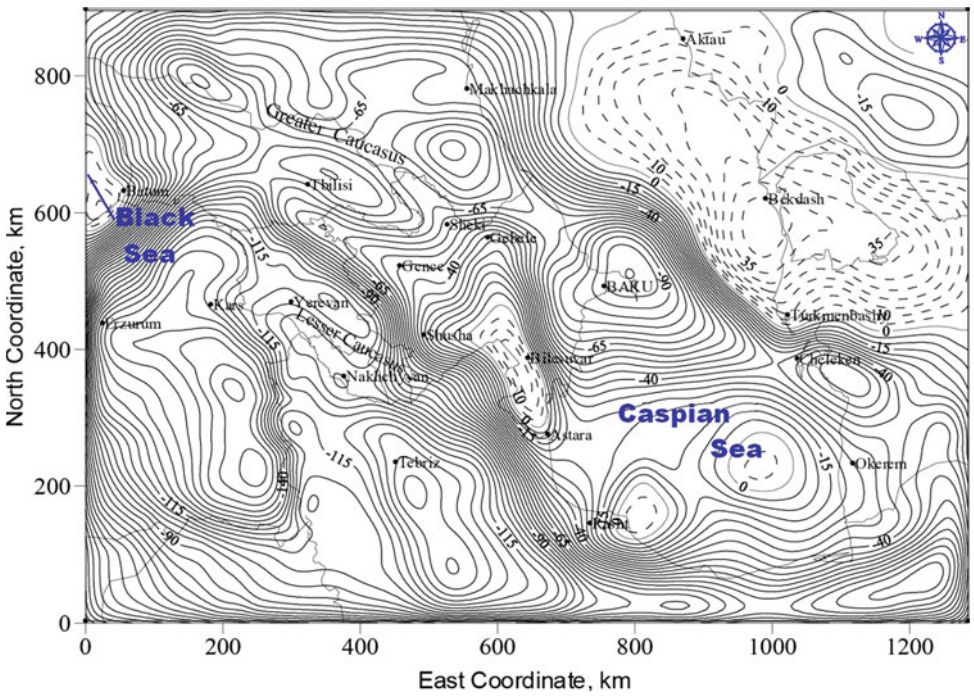

Fig. 4.27 Distribution of gravity field in the Caucasian-Caspian region upward continued to altitude of 20 km. Isolines density: 5 mGal (Kadirov 2004)

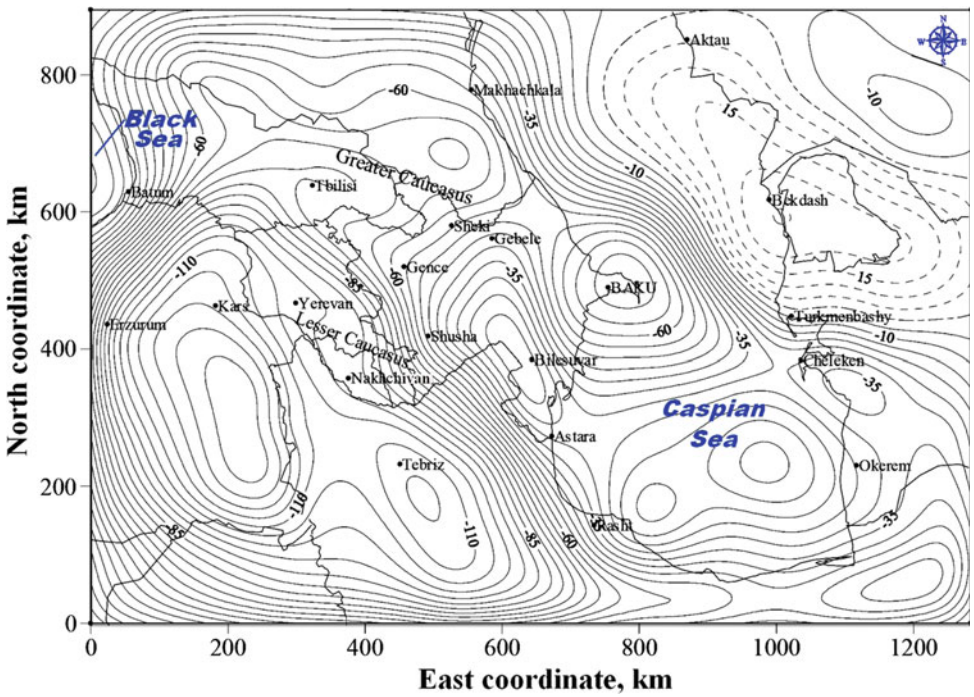

Fig. 4.28 Distribution of gravity field in the Caucasian-Caspian region upward continued to altitude of 50 km. Isolines density: 5 mGal (Kadirov 2004)

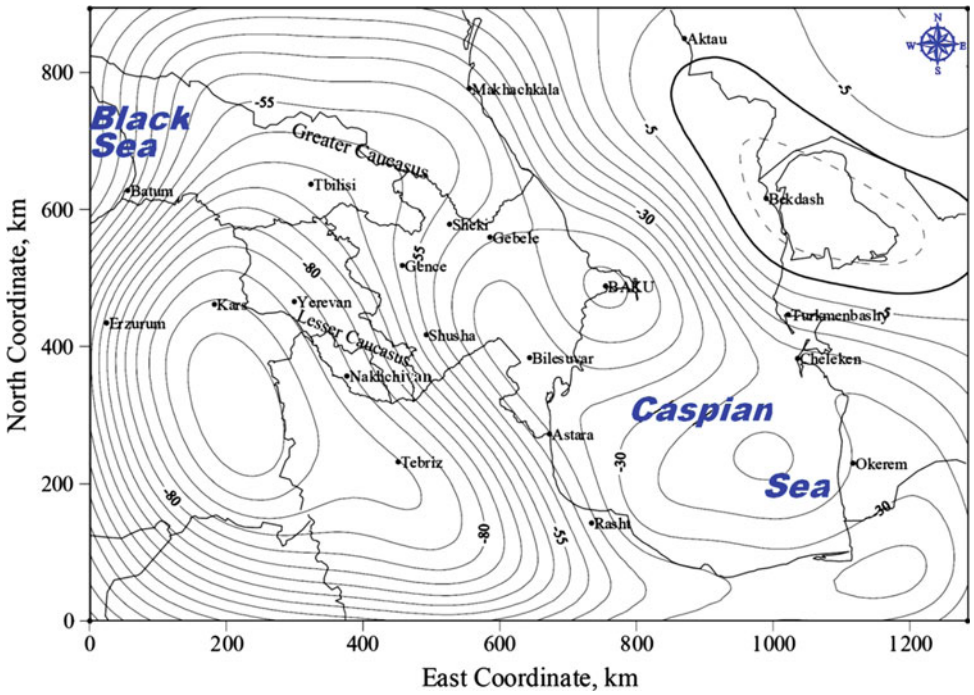

Fig. 4.29 Distribution of gravity field in the Caucasian-Caspian region upward continued to altitude of 50 km. Isolines density: 5 mGal (Kadirov 2004)

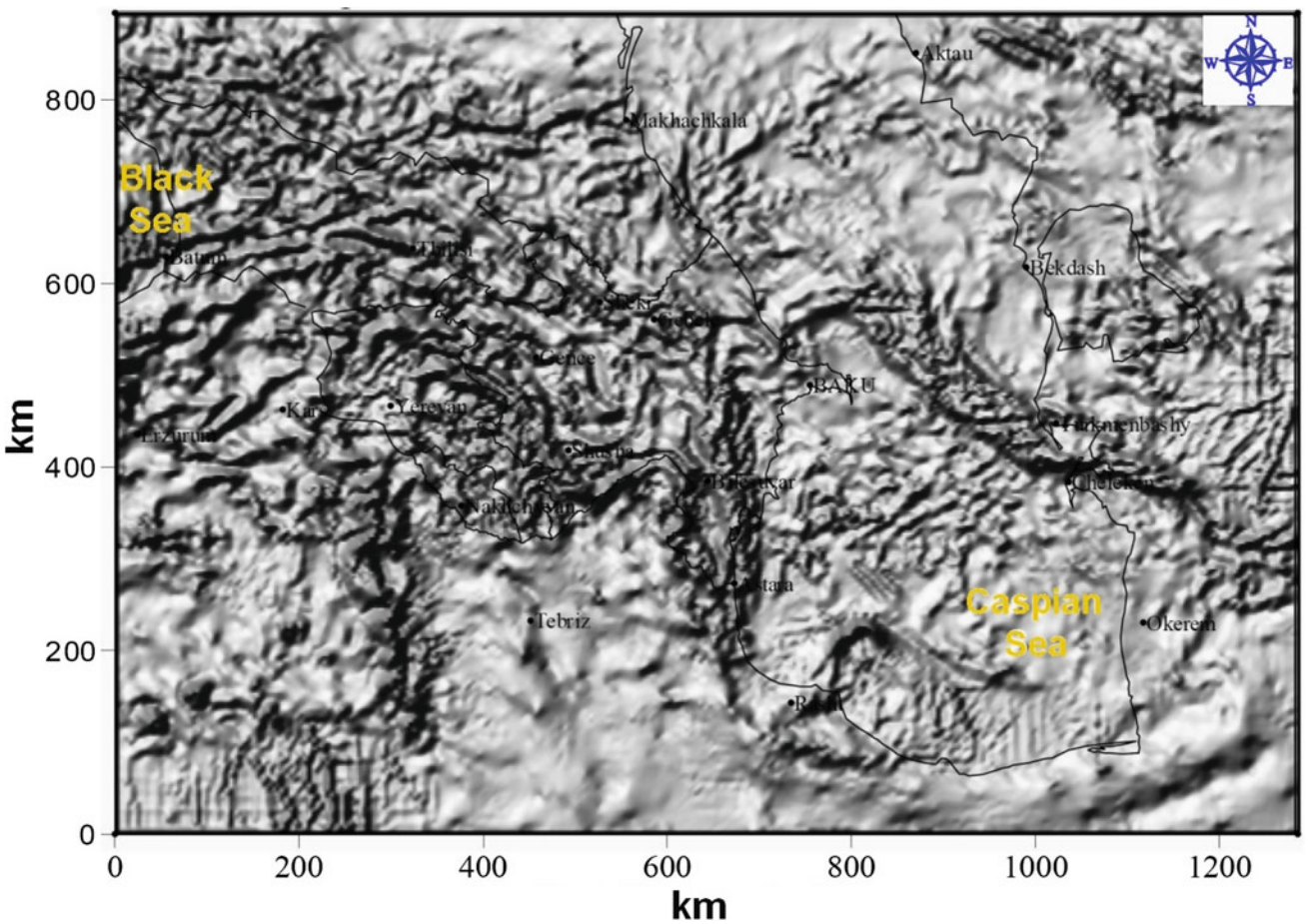

Fig. 4.30 Shaded relief map of total horizontal gradients of gravity field in the Caucasian-Caspian region upward continued to altitude of 20 km (horizontal and vertical light position angles were taken as 135° and 45°, respectively) (Kadirov 2004)

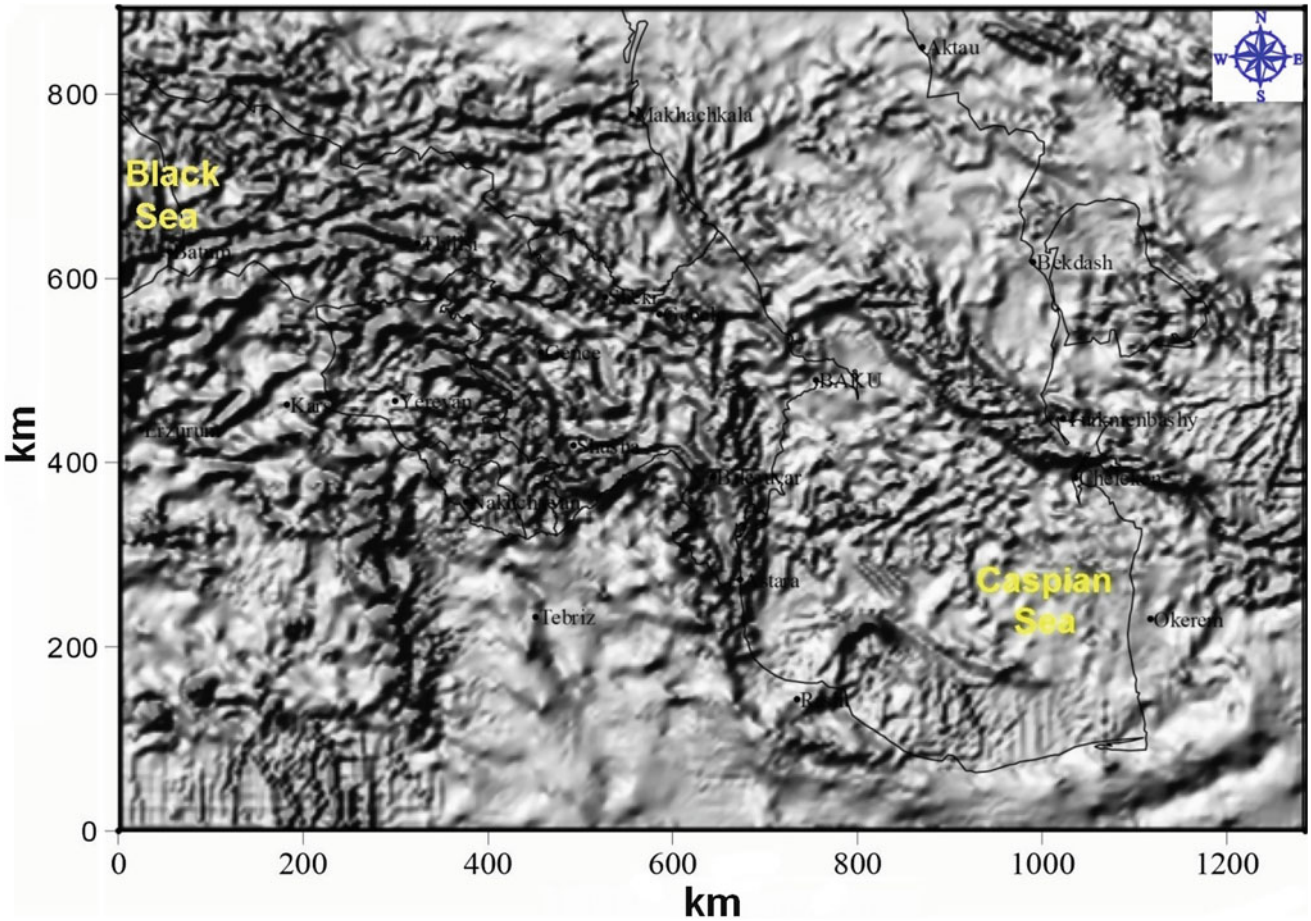

Fig. 4.31 Shaded relief map of total horizontal gradients of gravity field in the Caucasian-Caspian region upward continued to altitude of 20 km (horizontal and vertical light position angles were taken both as 45°) (Kadirov 2004)

regions with different signs and intensity of the field are mainly singled out by maps of the initial field and the field on a number of levels of the upper semi-space incorporating local and difference anomalies. Field region boundaries and other linear elements are traced by horizontal gradients and predominant strike isoline maps using the initial field and regional-anomaly maps and employing local elongated anomalies from corresponding charts. The local anomalies are singled out by maps of local and difference anomalies on the basis of the horizontal gradient map. These together give an idea of the depth extension of the sources.

4.3 Quantitative Analysis and Regioning

To enhance reliability when calculating the anomalous object parameters, techniques that measure different individual elements of the anomaly or the curve as a whole should be applied jointly. These include the methods of interpolation selection, singular points, analytical continuation, and selection based on approximation optimization. The optimum combination is determined by the specific nature of the region under survey and the nature of the material. For example, the density of the observation network and the accuracy of the field measurements impose certain restrictions on the method of singular points. The results of this method also depend on the noise fields of the sources occurring above the singular points of the objects being localized.

The applicability of methods under rugged terrain relief is not, in most cases, a decisive one if the observed anomaly is initially converted into a horizontal or inclined plane. The need for anomaly reduction is determined by the chosen set of techniques.

A system of advanced potential and quasi-potential geophysical field interpretation has been presented in Khesin et al. (1983, 1996), Eppelbaum and Khesin (2012) and

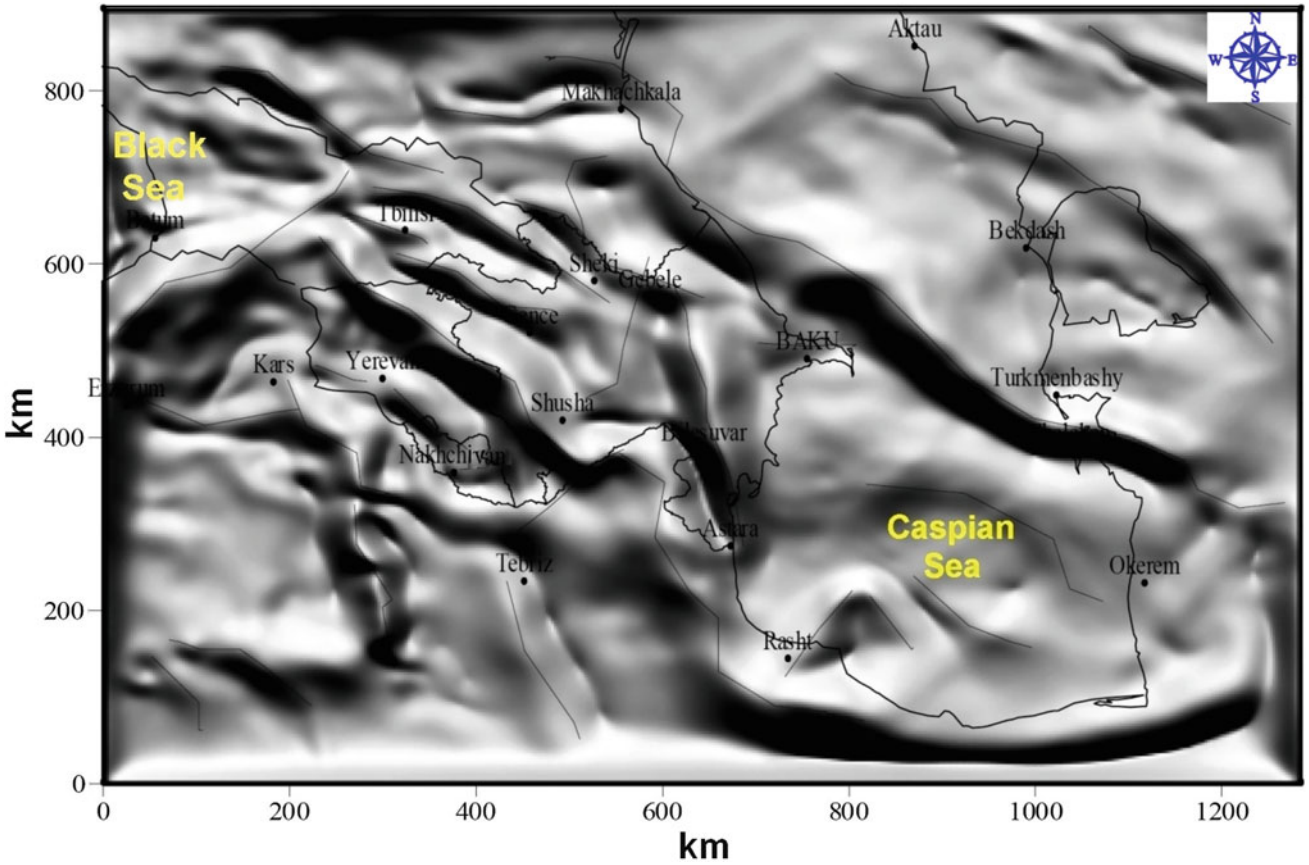

Fig. 4.32 Shaded relief map of full horizontal gradients of gravity field in the Caucasian-Caspian region upward continued to altitude of 50 km (horizontal and vertical light position angles were taken for 45° and 50°) (Kadirov 2004)

Eppelbaum et al. (2014). A key element of this system is a quantitative analysis of magnetic anomalies in conditions of inclined relief, oblique magnetization, and unknown level of the normal magnetic field. Let us consider several examples of the magnetic anomaly interpretation in complex regions of Azerbaijan.

Figure 4.36a exemplifies the use of the tangent method and the method of characteristic points, whereas Fig. 4.36b presents the method of characteristic areas (for the inclined thin bed model) applied for airborne magnetic data analysis in the Big Somalit area (northwestern Azerbaijan).

The Guton magnetic anomaly is situated in NW Azerbaijan (southern slope of the Greater Caucasus), near the border with Russia (Fig. 4.37). A detailed quantitative interpretation of this anomaly was carried out along fifteen profiles crossing this anomaly. The results along one of these profiles (the anomalous body was approximated by a thick inclined bed) are shown in Fig. 4.38 (here, improved tangent, characteristic point, and areal methods were applied). The methodology is described in detail in Khesin et al. (1996). The data indicate that the anomalous body is characterized by comparatively low magnetization (250 mA/m), considerable vertical thickness (about 30 km), and a steep dip of the lateral contacts. Analytical continuation and singular point methods applied on the same profiles gave similar results (Fig. 4.39). The characteristics of this anomalous body testify to the intermediate-acid composition of this target (intrusion). The interpretation of the significant vertical thickness of this body agrees with the geothermic data on the depth of the Curie discontinuity in this area (about 30 km) (Eppelbaum et al. 2014).

The outcroppings at the Earth's surface formed subvolcanic and subintrusive bodies of different consistencies which are apparently fragments of this large magmatic massif penetrating the upper part of the section along the extended faults of the common Caucasian direction. This

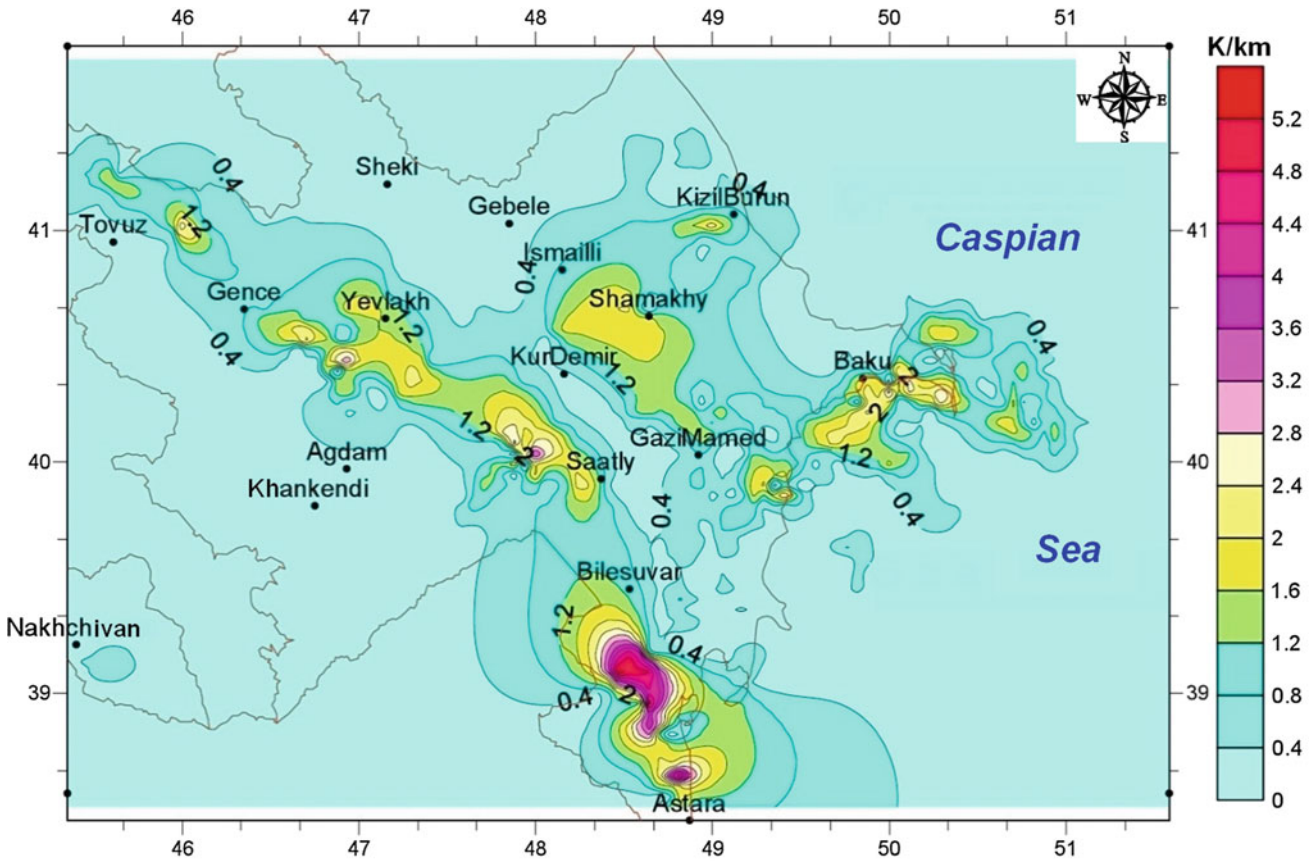

Fig. 4.33 Map of the total horizontal gradients of temperature field for Azerbaijan (for the depth of 5 km (Mukhtarov 2012)

magmatic focus is associated with the rich pyrite–polymetallic deposits of the Belakan-Zagatala ore field and possibly other areas in the Greater Caucasus (Ismailzadeh et al. 2005; Eppelbaum and Khesin 2012).

4.4 Compilation of Final Geophysical–Geological Maps

To delineate the ore mineralization associated with intrusive magmatism, the structures shown in Fig. 4.40 are especially instructive. They are presented as series of local anomalies corresponding mainly to the basic phases of granodiorite intrusive bodies.

The complex geological structure of Azerbaijan governs its highly intricate gravity and magnetic fields which reflect the effects of outcropped and deeply buried bodies and structures. Thus, to identify anomalies arising from a range of geological sources, both the observed geophysical fields and their various transformations must be used. Therefore, the legend of such a deep structure map must include a classification of spatial features (regional and local anomalies), geomorphological features (isometric anomalies, elongated anomalies, or ledges), and the signs and intensities of geophysical fields.

The regional minima of the same component outline the prospective oil and gas regions. The lower density of the Cenozoic terrigenous rock masses (2.0 ÷ 2.3 g/cm^3) unambiguously defines the regions of lower density at depth (gravity minima) as having the largest accumulation of sedimentary rock masses. The latter are promising as regards oil and gas resources in the Palaeogene–Miocene and Pliocene–Quaternary deposits. These regions are characterized by the conjunction of the Guba-Khachmaz and Iory-Agrichay zones with the Kobustan-Lower Kur zone in the east, and the Evlakh-Agjabedi zone (negative field regions 1, 5, 6, and 14, respectively, in Fig. 4.41).

The regioning scheme of the gravitational field in Azerbaijan as compared to the regional steps of the magnetic field is shown in Fig. 4.41. Regional peculiarities of the gravitational

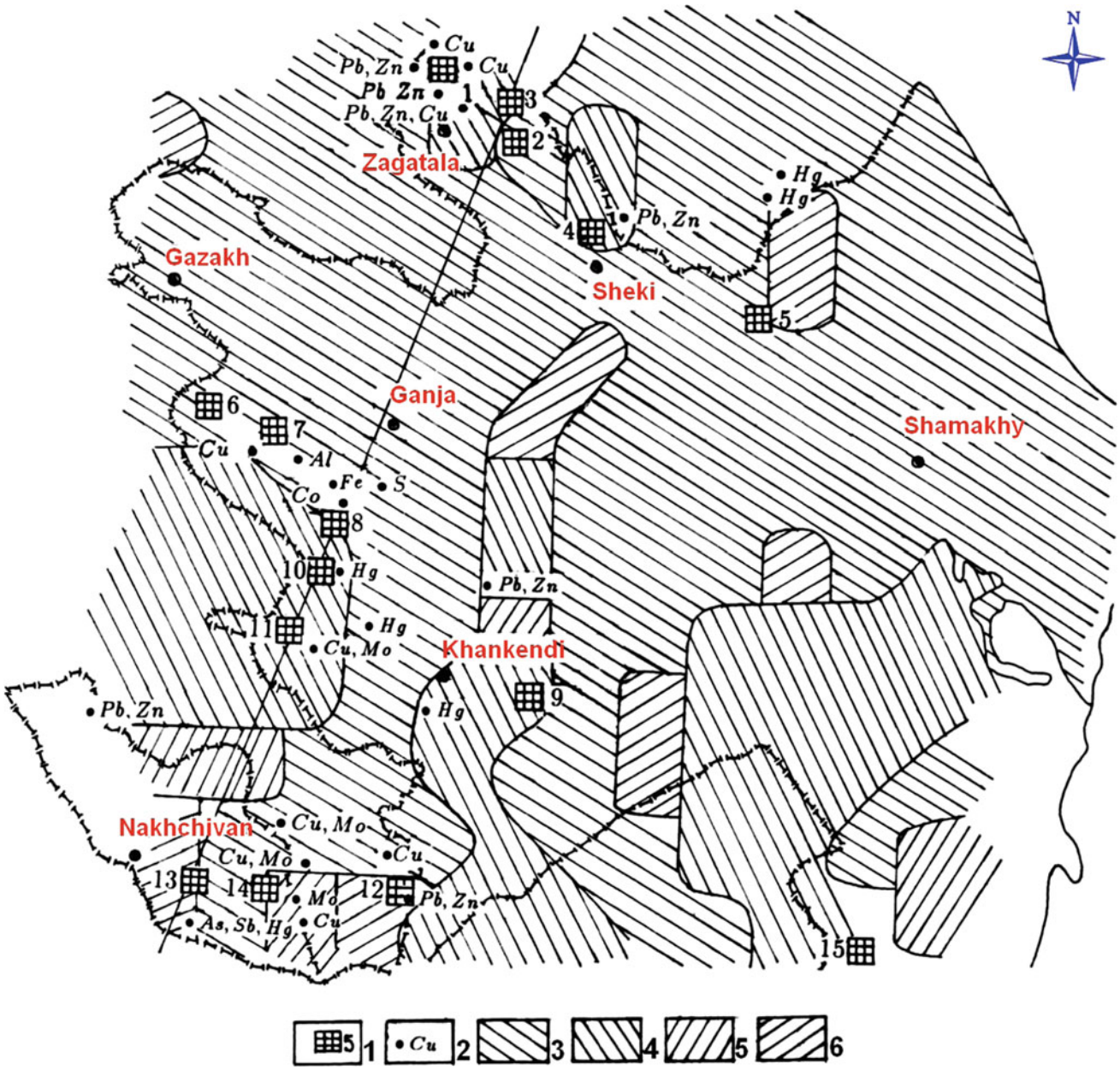

Fig. 4.34 Test well drilling site pattern in mountainous regions of Azerbaijan (after Khesin et al. 1996, with small modifications). (*1*) sites recommended for test well drilling and their numbers; (*2*) ore deposits; predominant courses of terrain relief isohypses: (*3*) WNW, (*4*) NNW, (*5*) NNE, and (*6*) ENE

and magnetic fields determine the regional factors of both oil and gas and ore control. The Shamkir-Gedabey-Dashkesan ore zone and the Mekhmana ore district (Lesser Caucasus), and the Belakan-Zagatala ore field (Greater Caucasus) which were identified on the basis of systematic geophysical studies, as well as the Kutkashen-Ismailly district (the Greater Caucasus), which has potential endogenic mineralization according to a number of indicators (Azizbekov et al. 1972; Eppelbaum and Khesin 2012), are controlled by the positive difference field $\Delta g_{B(8-20)}$ (see Fig. 4.15) that corresponds to zones 8 and 2, respectively, as shown in Fig. 4.41.

Accumulated experience shows the importance of performing independent regioning using initial field and regional-anomaly maps. Comparing the results in a unified

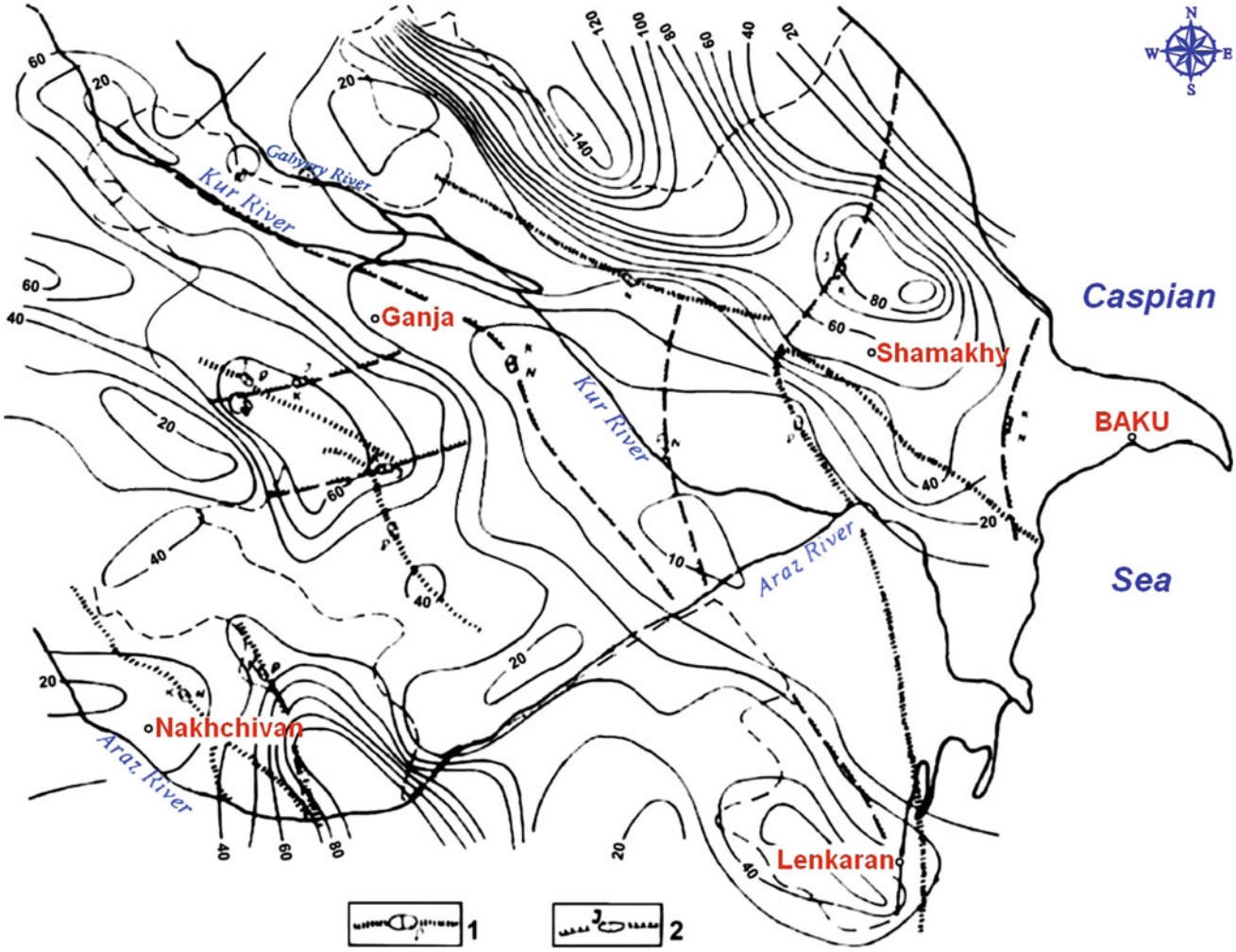

Fig. 4.35 Map of equal lengths of isohypses for the topography of Azerbaijan (after Khesin et al. 1996). (*1*) deep fault (*dots* show buried paths of the fracture); (*2*) flexures (on the surface as shown by *solid lines* and buried as shown by *dashed lines*); indices point to the expected section interval dissected by fractures

scheme makes it possible to determine common features and differences in deep structure elements and in the upper portion of the section, and reveal the elements (primarily, disjunctive dislocations, and blocks) that manifest themselves at the different structural stages.

The transforms reflecting the degree of heterogeneity of the field such as anomalous coefficients, dispersion, and entropy are the most useful for singling out field areas in open regions. In different areas, these parameters can take on different geological meanings. They are also appropriate for solving more specific problems, in particular in the regioning of separate portions by the degree of heterogeneity of their lithological complexes. Here, it makes sense to compute the specific sinuosity of the isolines.

The map of gravity–magnetic anomalies (Fig. 4.42) shows both these minima since the problem of their nature can be solved at the stage of anomaly examination (Alexeyev et al. 1989; Eppelbaum and Khesin 2012).

A description of gravity anomalies was based on the following: (1) difference fields ("ring" anomalies) $\Delta g_{B(8-20)}$ and $\Delta g_{B(4-10)}$ computed as the difference between upward continued fields in the Bouguer reduction (terrain correction

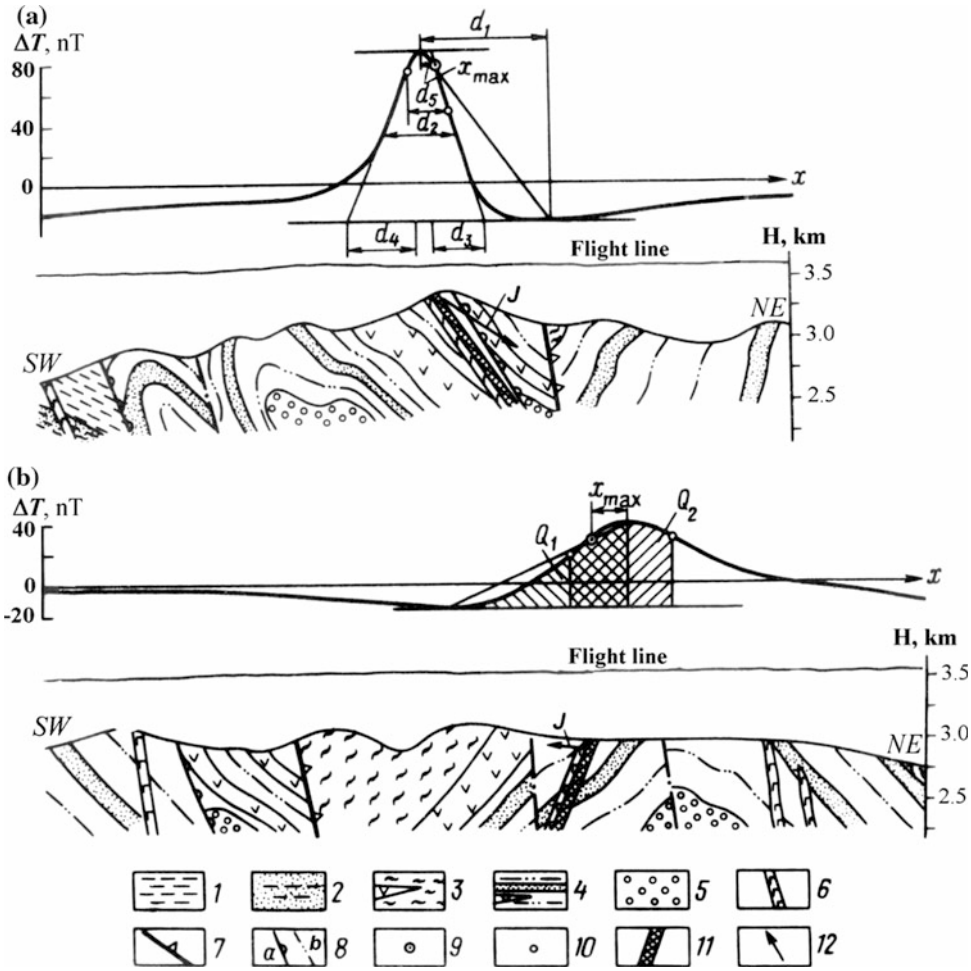

Fig. 4.36 Examples of quantitative interpretation of ΔT plots along profiles 171 (**a**) and 181 (**b**) in the area of the Big Somalit (southern slope of the Greater Caucasus) (Khesin et al. 1996). (*1*) Yalakhkam suite J_2aal_2; (*2*) Zainkam suite J_2aal_1; (*3*) Nagab suite J_1toa_3; (*4*) Tseilakhan suite J_1toa_3; (*5*) the Lower and Middle Toarcian suite J_1toa_{1-2}; (*6*) dikes of the gabbro–diabasic association; (*7*) the Main Caucasian upthrust–overthrust; (*8*) ore controlling (**a**) and ore distributing (**b**) upthrust–overthrusts; (*9*) Reford's point; (*10*) inflection points; (*11*) anomalous body according to the interpretation results; (*12*) obtained direction of the magnetization vector

was computed with a radius of 200 km, and the density of the intermediate layer was defined as 2.67 g/cm^3) at heights of 8 and 20, 4 and 10 km, respectively, (2) the residual field $\Delta g_{B(0-4)}$(local anomalies were calculated as the difference between the initial land Bouguer gravity and this field continued upward to a height of 4 km), and (3) horizontal gravity gradient field at a height of 2 km ($\Delta g_{x(2)}$).

These features were analyzed on the basis of the following descriptors.

I. The residual field $\Delta g_{B(0-4)}$ in the mountain-folded regions reflects the influence of near-surface Alpine structures composed of volcanogenic and volcanogenic–sedimentary associations, and intrusions (both outcropping to the Earth's surface and near-surface), and in the Kur Depression as regards the distribution of dense inhomogeneities of the upper part of the sedimentary floor.
II. The peculiarities of difference field ("ring" anomalies) $\Delta g_{B(8-20)}$ were described in Sect. 4.2.2.
III. Significant anomalies of $\Delta g_{x(2)}$ should be taken into consideration by delineation and examination of regional gravity anomalies.

These descriptors were determined on the basis of analysis of petrophysical parameters (see Sect. 4.1) as well as data on density of metamorphic foundation outcropped in Armenian territory.

According to Nikolsky et al. (1975), basement outcrops in Armenia are characterized by the following average density values: Aparan (2.80 g/cm^3), Arzakan (2.76 g/cm^3), Lok (2.76 g/cm^3), Eranos (2.87 g/cm^3), Nyuvadi (2.80 g/cm^3), and Akhum (2.63 g/cm^3). It should be noted that the Shamkir (Beyukkishlak) protrusion, located in Azerbaijanian territory 20 km east of Akhum, is also characterized by an average density of 2.63 g/cm^3.

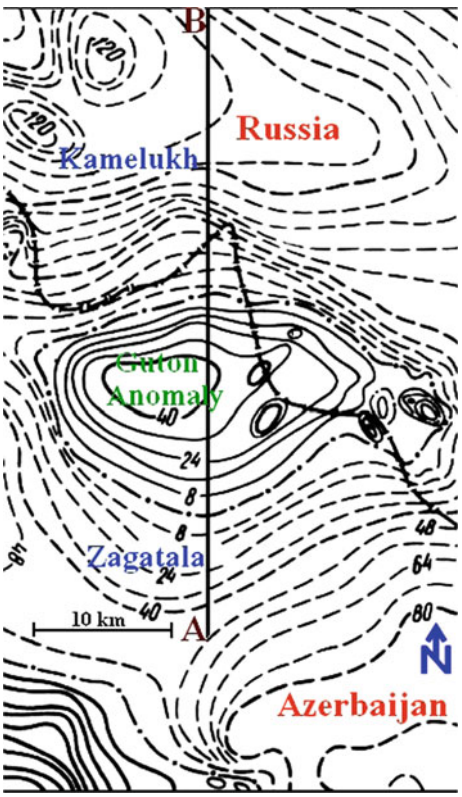

Fig. 4.37 Guton magnetic anomaly (results of an airborne survey) on the southern slope of the Greater Caucasus. The map shows the total magnetic field ΔT (isolines are given in mA/m) and the location of interpreting profile **A–B** (Eppelbaum and Khesin 2012)

At the same time, the density of separate types of rocks composing these protrusions may vary considerably. For instance, muscovite and sericite–quartz shales have a density of 2.66 (Aparan) to 2.79 g/cm^3 (Lok), quartzite from 2.60 (Lok) to 2.67 g/cm^3 (Nyuvadi), phyllite from 2.63 (Akhum) to 2.84 g/cm^3 (Arzakan), greenstone rocks (plagioclase porphyrites, tuff-sandstone, etc.) from 2.71 g/cm^3 (Lok) to 2.83 g/cm^3 (Aparan), gneisses from 2.60 g/cm^3 (Arzakan) to 2.94 g/cm^3 (Nyuvadi), limestone and marble from 2.66 g/cm^3 (Aparan) to 2.78 g/cm^3 (Arzakan), and amphibole shales from 3.00 g/cm^3 (Aparan) to 3.03 g/cm^3 (Eranos).

In the Shamkir (Beyukkishlak) cericite-muscovite-graphite outcrop, shales were found with comparatively low density (which is typical for the average density of the Baikalian series) (Azizbekov et al. 1972). An analogical situation was identified on the Akhum outcrop where at the Earth's surface, phyllite clay shales representing the less metamorphosed part of the geological section were identified (Nikolsky et al. 1975). Thus, despite this variability in density, the average density of the rocks composing the pre-Alpine foundation in SW Azerbaijan can be estimated as 2.80 ± 0.05 g/cm^3.

For the Armenian territory, the regional gravity map $\Delta g_{B(reg)}$ was constructed by a methodology that included using points of outcropped metamorphic basement (6 points), boreholes that crossed the basement (7 points), and other data. This map as a whole coincides with the $\Delta g_{B(8)}$—map obtained by analytical continuation of the surface gravity field to a height of 8 km (the absolute levels of these maps are different) (Sirotkina and Nikolsky 1971). It can be suggested that analogical correspondence is correct and for the Lesser Caucasian part of Azerbaijan territory. Thus, the $\Delta g_{B(8)}$ map mainly reflects the variations of the upper surface and inhomogeneities of the consistency in the pre-Alpine metamorphic floor and deeper layers of the Earth's crust; the effects of the Alpine floor are weakly present in this map. Therefore, the difference field $\Delta g_{B(8-20)}$ ("ring anomalies") primarily reflects the influence of the internal structure and inhomogeneities of the consistency of Baikalian and possibly the pre-Baikalian floor. In addition, as regards the transition from the Lesser Caucasus to depression regions, the difference field mainly represents the structure and consistency of the Mesozoic associations which act here as a dense basement.

Thus, the anomalies in the $\Delta g_{B(0-4)}$ map indicate local (close to the Earth's surface) objects; anomalies recognized in the $\Delta g_{B(8-20)}$ map represent some regional (deep) objects. The $\Delta g_{B(4-10)}$ map has a pattern similar to $\Delta g_{B(8-20)}$, but with a more differentiated field.

To examine regional magnetic anomalies, the following measures were used: field ΔT (in the Middle Kur Depression —field Z_a) at 6 and 10 km and the $\Delta T(Z_a)$ horizontal gradient field at 2 km. Attempts to reveal local magnetic anomalies as a residual field of $\Delta T_{(0-6)}$ or $\Delta T_{(0-10)}$ were unsuccessful because of the considerable difference in the observed magnetic field in the Lesser Caucasus. Therefore, local magnetic anomalies were selected directly in the initial field, and magnetic maxima were singled out irrespective of whether they were found in a positive or negative field. Magnetic minima were identified in a similar fashion. Some of these minima were conjugated with the corresponding maxima in relation to the oblique magnetization typical of the Azerbaijan territory. Other minima corresponded to objects with a low magnetization or reversely magnetized targets.

In the $\Delta g_{B(8-20)}$ map intensive (first tens of mGals) and extended (first hundreds of km) gravity, ledges were identified that split the areas of positive and negative field. Similar ledges were identified in the $\Delta g_{B(4-10)}$ map. The intensive linear

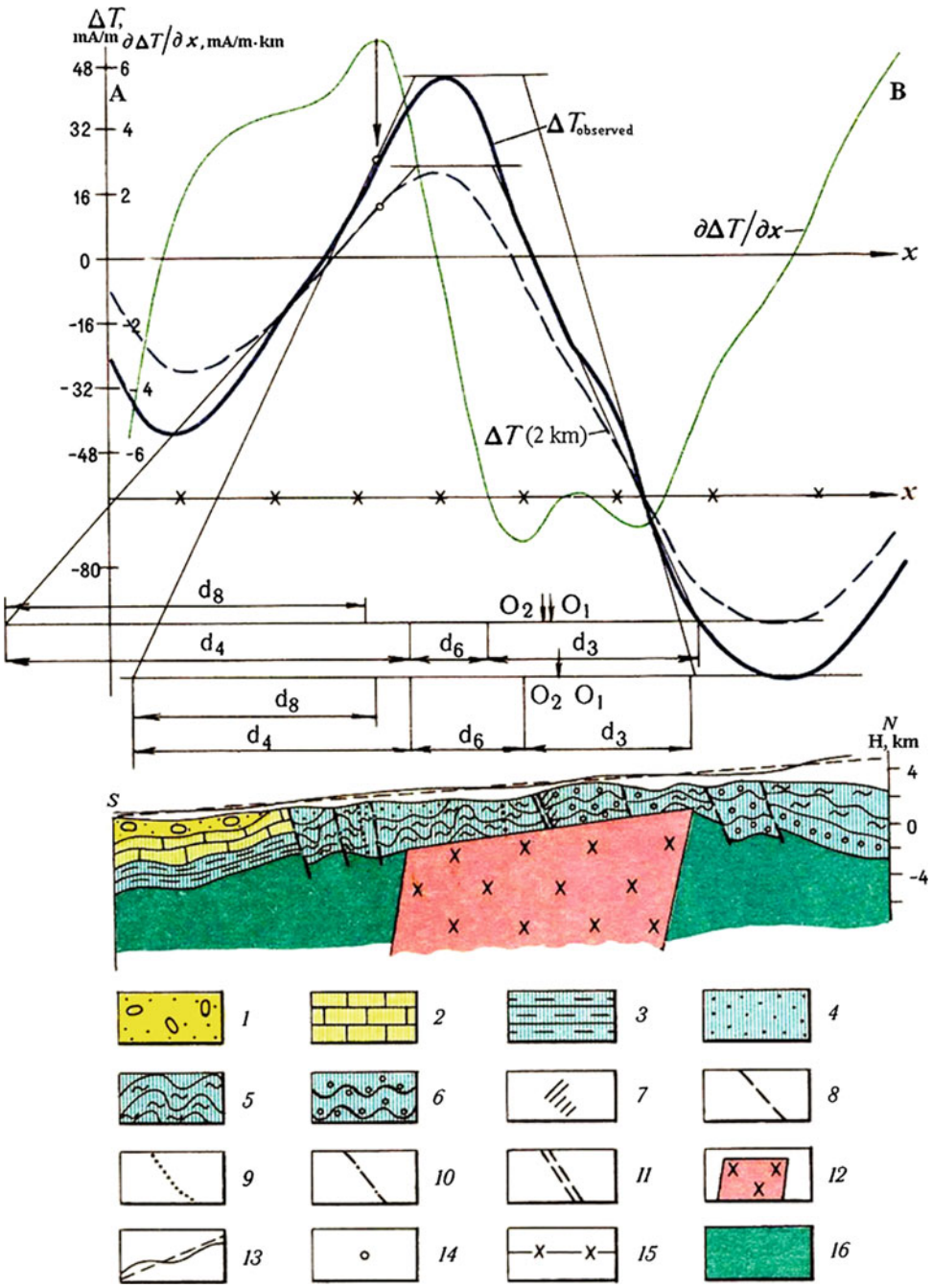

Fig. 4.38 Interpretation of ΔT graphs on two levels along profile 28 through the Guton anomaly (southern slope of the Greater Caucasus) (Khesin et al. 1996). (*1*) recent alluvial deposits; (*2*) limestones, tuff sandstones, clay shales (*K*); (*3*) mudstones, tuff sandstones (J_3); (*4*) monolith clay shales and coarse-grained tuff sandstones (J_2); (*5*) sandy-clay shales with horizons of sand flysch, metamorphosed clay shales, and sandstones (J_2); (*6*) phyllitizated clay shales, sandstones, spilites (J_1); (*7*) dikes and sheet bodies of the gabbro–diabasic association (J_2); (*8*) regional upthrust–overthrusts; (*9*) upthrust–overthrusts separating the longitudinal tectonic steps of the second order; (*10*) upthrust–overthrusts complicating the longitudinal tectonic steps; (*11*) transverse fractures; (*12*) magmatic intrusion of intermediate-acid composition according to the interpretation data (in non-segmented $J_{1–2}$ complex); (*13*) the lines of flight and averaging inclined *straight line*; (*14*) inflection point of the plot ΔT nearest to the maximum on the *left*; (*15*) corrected zero line of the plots ΔT; O_1 and O_2 are locations of the origin (middle of the anomalous body's upper edge) obtained from $x_{un–r}$ to $x_{un–l}$, respectively; (*16*) $J_{1–2}$ complex

maxima or minima correspond to them in the horizontal gravity gradient map. Axes of these ledges are shown in the map of gravity–magnetic anomalies (Fig. 4.42) as two bold colored lines: brown from the side of the positive field and green from the side of negative one; arrows in the green line are oriented toward the block of lesser density. Less intensive (several mGals) and less extended gravity ledges are represented by an analogous symbol with lines of less density.

Regional magnetic steps were identified by analysis of $\Delta T_{(10)}$ and $Z_{a(10)}$ maps by taking into consideration the map of the horizontal magnetic gradient $\Delta T(Z_a)$ at 2 km. Axes of these ledges are depicted in this map (Fig. 4.42) as two bold colored lines: Blue is from the side of positive field, and red is from the side of negative field; arrows on the red line are oriented toward the side of the block with lesser magnetization (Eppelbaum and Khesin 2012).

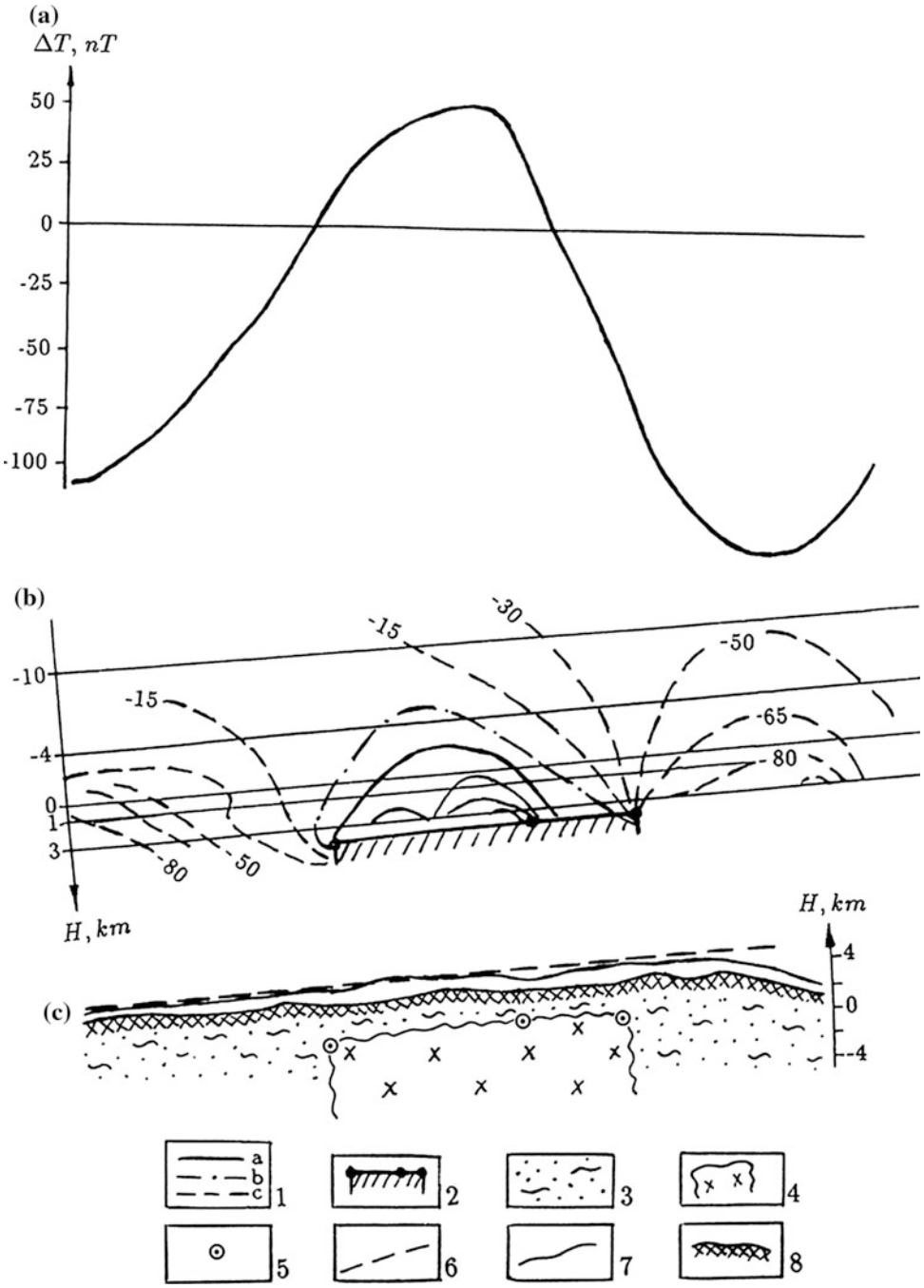

Fig. 4.39 Example of interpretation of the Guton anomaly implementing analytical continuation and singular point methods (Eppelbaum and Khesin 2012). **a** plot of ΔT; **b** an isoline chart based on the results of analytical continuation in an inclined half-space; **c** a schematic section of the anomalous object. (*1*) isolines, nT: **a**—positive, **b**—zero, **c**—negative; (*2*) magmatic intrusion of an intermediate-acid composition (according to the interpretation results); (*3*) the upper edge of the anomalous object, obtained by the method of analytical continuation (*black points* show logarithmic peculiarities of the field); (*4*) singular point; (*5*) inclined straight line approximating the observation profile

Regional gravity maxima and minima (with intensity up to 20 mGals) as revealed in the $\Delta g_{B(8-20)}$ map are contoured by the points with values approximately equal to half the extremal values.

In the map (Fig. 4.42), they are shown as solid bold brown (maxima) and green (minima) lines, respectively, with arrows oriented to the side of decreasing field. Within certain contours are located several (1 to 3–4) anomalies of $\Delta g_{B(4-10)}$ but are not shown to make the map pattern more legible.

Local gravity and magnetic maxima indicated, respectively, in maps $\Delta g_{B(0-4)}$ and $\Delta T\,(Z_a)$ are represented by points with the half maximum of the corresponding extremum. The

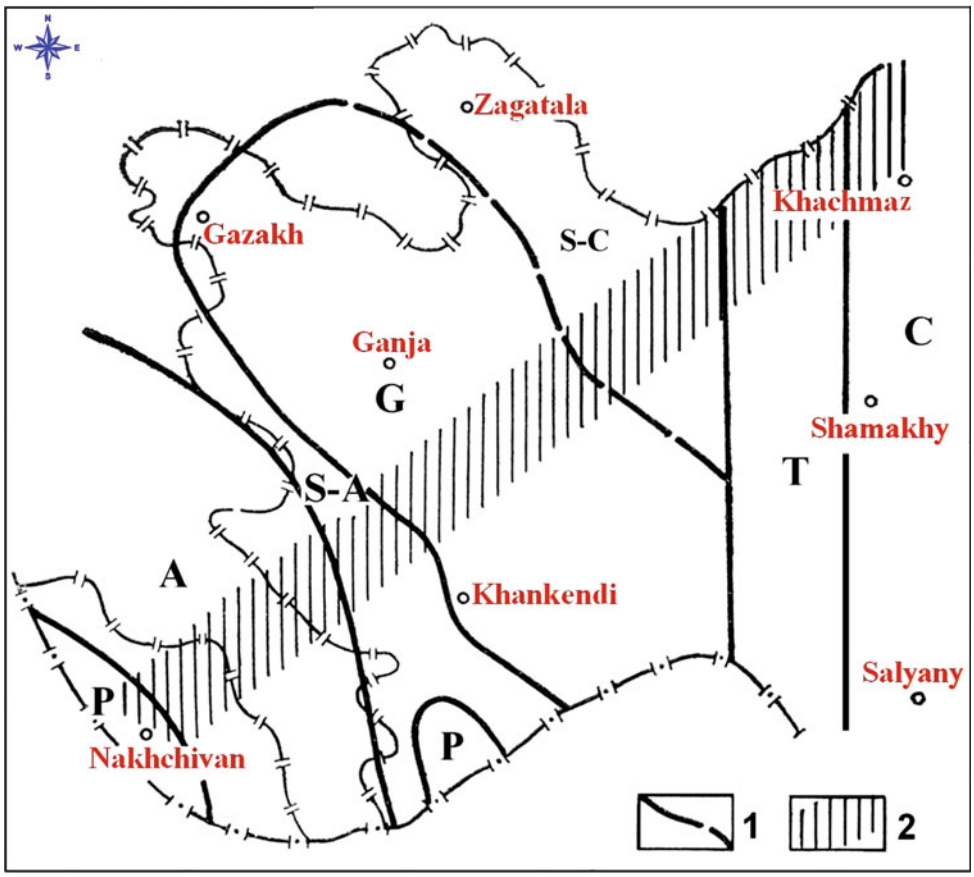

Fig. 4.40 Geophysical data of the Azerbaijan tectonic regioning (after Khesin et al. 1996). (*1*) boundaries of tectonic units, (*2*) the largest zone of anti-Caucasus dislocations delineated in most geophysical maps

maxima and minima are divided into intensive (exceeding the absolute value of 3–4 mGals and 300–400 nT) and less intensive (intensity of 1–2 mGals and 100–200 nT).

In the map (Fig. 4.42), intensive local gravity maxima are depicted by the dense dark shading surrounded by a brown line, and intensive minima are indicated by the dark green line. Less intensive local gravity maxima in a positive field are shown by light brown shading contoured by a brown line; the same maxima in a negative field are represented by light brown shading surrounded by a green line. Similarly, less intensive gravity minima are shown by light green shading surrounded by a green line in a negative field and a brown line in a positive field.

A similar system of symbols was applied to depict local magnetic anomalies: Intensive maxima are shown by dark blue shading surrounded by a blue line in a positive field and red in a negative field. The less intensive maxima are shown by light blue shading surrounded by blue or red lines depending on the sign of field in which the maximum appears. The local magnetic minima are shown as dark or light red shading depending on field intensity and a red or blue contour line depending on the sign of surrounding field.

The points of high intensive magnetic maxima and minima (exceeding 2000 nT in absolute value) are presented, respectively, by a blue cross and a bold red dot (imitating the tail and head of an arrow—magnetization vector).

Fig. 4.41 Comparison of gravity field regioning and regional steps of magnetic field mapping (after Khesin et al. 1996). (*1*) Axes of intense extended gravity steps distinguished in the $\Delta g_{B(8–20)}$ and $\Delta g_{B(4–10)}$ difference fields and the horizontal gradient field obtained from Δg_B at a level of 2 km; (*2*) axes of marked gravitational steps distinguished in the same fields; (*3*) axes of regional magnetic steps distinguished in the magnetic field at a level of 10 km and in the field of its horizontal gradient at a level of 2 km; (*4*) $\Delta g_{B(8–20)}$ positive gravity field blocks and zones; (*5*) $\Delta g_{B(8–20)}$ negative gravity field blocks and zones; (*6*) weak boundaries of $\Delta g_{B(8–20)}$ positive or negative gravity field areas; (*7*) gravitational step number (beginning and end of a step are indicated); (*8*) magnetic step number; (*9*) number of $\Delta g_{B(8–20)}$ positive or negative gravity field zones and blocks. *Note* The *arrows* on the symbols show the direction to the blocks of lower density or magnetization

The areas or intersections of local gravity and magnetic anomalies are shown by combined symbols: strips of corresponding color and shading intensity oriented in a NE direction at an angle of 45°.

On the basis of a combined analysis of gravity and magnetic fields, selected areas for deep drilling were charted (Fig. 4.43).

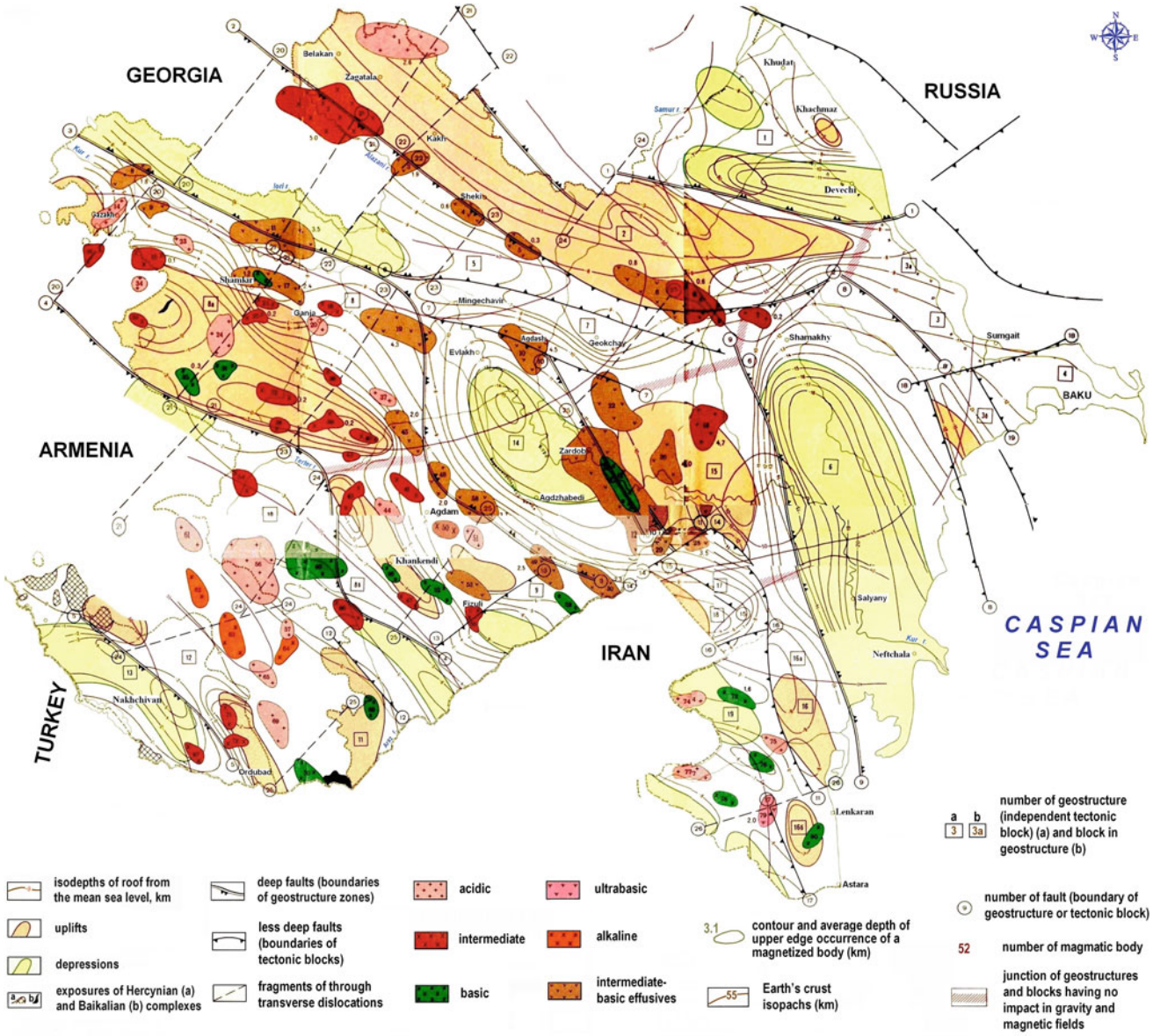

Fig. 4.42 Map of the deep structure of Azerbaijan with its adjacent regions according to gravity and magnetic data (after Alexeyev et al. (1989); Eppelbaum and Khesin (2012) with small modifications, geology after Azizbekov et al. (1972)

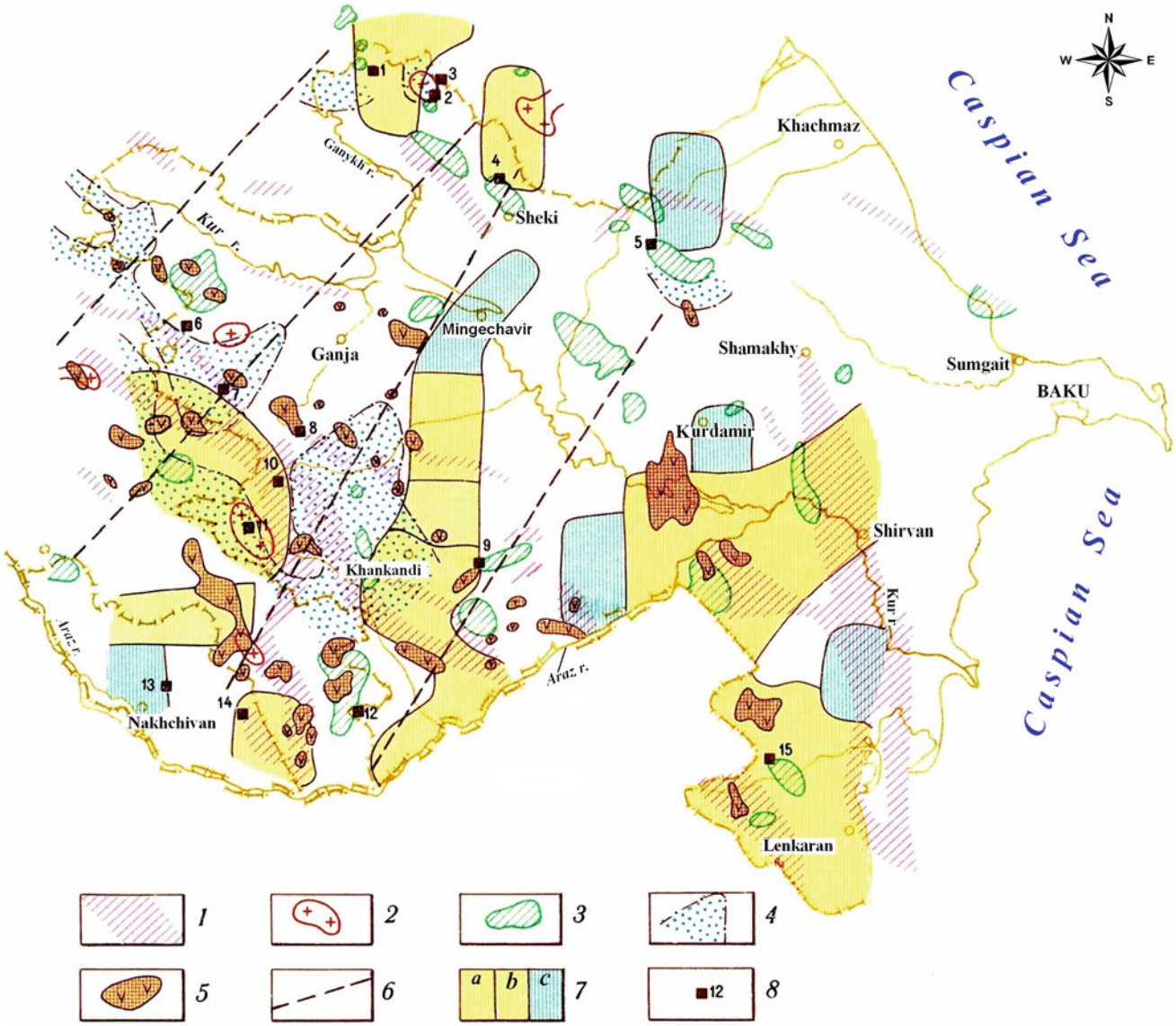

Fig. 4.43 Location of areas for deep drilling in Azerbaijan derived from integrated examination of geophysical fields (Khesin et al. 1996; geology is mainly from Azizbekov et al. 1972). (*1*) Zones of large faults detected by the use of the highest gradients of the gravity field in the Bouguer reduction, (*2*) acid intrusions revealed by negative local gravity anomalies, (*3*) dome-shaped structures or areas of basic rock development revealed by positive local gravity anomalies, (*4*) uplifts of basic and middle magnetized generations found after determination of singular points in the reference aeromagnetic net, (*5*) areas of basic rock development corresponding to local magnetic anomalies, (*6*) transversal faults marked by local magnetic anomalies, (*7*) neotectonic blocks corresponding to areas with anomalous (different from common Caucasian) strikes of relief isolines: **a**—NNW, **b**—NNE, and **c**—NEE, and (*8*) areas of recommended reference boreholes and their numbers

References

Aksyonovich, G.I., Aronov, L.E., Galperin, E., Kosminskaya, I.P. and Gegelgants, A.A., 1962. *Deep Seismic Sounding in Central Part of the Caspian Sea*. USSR Academy of Sciences, Moscow, (in Russian).

Alexeyev, V.V., Gadjiev, T.G., Karkoshkin, A.I. and Khesin, B.E., 1989. *Gravity and Magnetic Anomalies of Azerbaijan and Their Geological Interpretation*, (Ismailzadeh, T.A. and Khesin, B.E., Eds.), Printing Map Factory, Leningrad (in Russian).

Aliyev, Ch.S., Feyzullayev A.A. Valsangiacomo, C., Hoffmann, M., Baghirli, R.J. and Veliyeva, F.F., 2012. Radon problem in Azerbaijan: results of indoor measurements and its nature. In: (Alizadeh, Ak.A., Ed.), *Modern Problems of Geology and Geophysics of the Caucasus*. Nafta-Press, Baku, 52-71.

Aliyev, Ch.S. and Zolotovitskaya, T.A., 1996. Results of radiometric investigations. *In*: (Kerimov, K.M., Ed.) *Geophysical Investigations in Azerbaijan*, Sharg-Garb, Baku, 386-389 (in Russian).

Aliyev, Ch.S. and Zolotovitskaya, T.A., 2000. Radioactivity of Eocene rock complexes in the Central Talysh. *Izvestiya, Acad. Sci. Azerb*., Ser.: Earth Sci., No. 1, 67-72.

Aliyev, Ch.S. and Zolotovitskaya, T.A., 2005. Comparison of gamma-field with geological structure, geophysical fields, oil&gas bearing, and seismicity. *In*: (Ak.A. Alizade, Ed.), *Geology of Azerbaijan*, Vol. **V**, Physics of the Earth, Nafta-Press, 292-312 (in Russian).

Aliyev, G.A., Akhmedbeyli, F.S., Ismailzade, A.D., Kangarli, T.H. and Rustamov, M.I. (Khain, V.E. and Alizadeh, Ak.A., Eds.), 2005a. *Geology of Azerbaijan*, Vol. **IV**: Tectonics. Nafta-Press, Baku (in Russian).

Aliyev, S.A., Mukhtarov, A.S., Bagirli, R.J. et al., 2005b. Geothermal studies in Azerbaijan. In: (Alizadeh, Ak.A., Ed.), *Geology of Azerbaijan.* Vol. V: *Physics of the Earth*. Nafta-Press, Baku, 229-263 (in Russian).

Aliyev S. et al. (2001) Radioactive fields of mud volcanoes of Azerbaijan. *Geophysics News in Azerbaijan*, **3**, 25-32.

Aliyev, S.A., 1988. Geothermal fields of depression zones of the South-Caspian Depression and their relation with oil and gas bearing capacity. *D.Sci. Thesis*, Geol. Inst. Azerb. Acad. Sci., Baku (in Russian).

Aliyev, S.A. and Aliyev, A.S., 1995. Heat flow in depression of Azerbaijan. In: (M.L. Gupra and M. Yamano, Eds.), *Terrestrial Heat Flow and Geothermal Energy of Asia*. Oxford & IBH Publishing Co. PVT. Ltd., New Delhi.

Aliyev, S.A. and Mukhtarov, A.S., 2000. Geothermal studies in the borehole. In: (Ak.A. Alizadeh, V.E. Khain and A.D. Ismailzadeh, Eds.) *Saatly Superdeep Well. Studies of Deep Structure of the Kur Intermountain Depression Based on Materials of Drilling of Saatly Superdeep Well SG-1*. Nafta-Press, Baku, 213-233 (in Russian).

Alizadeh, Ak.A. (Ed.). 2012. *Modern Problems of Geology and Geophysics of the Caucasus*. Nafta-Press, Baku.

Andreyev, B.A. and Klushin, I.G., 1962. *Geological Interpretation of Gravity Anomalies*. Gostoptekhizdat, Leningrad (in Russian).

Azizbekov, Sh.A., Alizadeh, K.A., Shikalibeyli, E.Sh. and Gadjiev, T.G. (Eds.), 1972. *Geology of the USSR*, *Azerbaijan*, Vol. **XLVII**, Nedra, Moscow (in Russian).

Beardsmore, G.R. and Gull, J.P., 2001. *Crustal Heat Flow: A Guide to Measurement and Modelling*. Cambridge, Cambridge Univ. Press.

Bhaskara Rao, D., 1986. Modelling of sedimentary basins from gravity anomalies with variable density contrast. *Geophys. J. R. Astron. Soc*., **84**, 1, 207-212.

Bhaskara Rao, D. and Ramesh Babu, N., 1991. A fortran-77 computer program for three-dimensional analysis of gravity anomalies with variable density contrast. *Comput. Geosci*., **17**, 655-667.

Bhattacharyya, B.K., 1966. Continuous spectrum of the total magnetic anomaly due to a rectangular prismatic body. *Geophysics*, **31**, 97-121.

Blakely, R.J., 1995. *Potential Theory in Gravity and Magnetic Applications*. Cambridge Univ. Press.

Borisov, A.A., 1967. *Deep Structure of the Territory of the USSR According to Geophysical Data*. Nedra, Moscow (in Russian).

Borovko, N.N., 1971. *Statistical Analysis of Spatial Geological Regularities*. Nedra, Leningrad (in Russian).

Dehghani, G.A. and Makris, J., 1983. The gravity field and crustal structure of Iran. *Geodynamic Project* (*Geotraverse*) *in Iran*. Final Report. 51. Geological Survey of Iran, 50-68.

Eppelbaum, L.V., 2012. Geophysical Studies in the Caucasus (1925 – 2012): Initial, Basic and Modern Stages. *Trans. of the 8th EUG Meet.*, Geophysical Research Abstracts, Vol. **14**, EGU2012-1341, Vienna, Austria, 1-3.

Eppelbaum, L.V., 2014. Estimating informational content in geophysical observations on example of searching economic minerals in Azerbaijan. *Izvestiya* (*Proceedings*), *Acad. Sci. Azerb. Rep.*, Ser.: Earth Sciences, Nos. 3-4, 31-40.

Eppelbaum, L. and Katz, Y., 2011. Tectonic-Geophysical Mapping of Israel and eastern Mediterranean: Implication for Hydrocarbon Prospecting. *Positioning*, **2,** No. 1, 36-54.

Eppelbaum, L.V. and Katz, Yu.I., 2015. Paleomagnetic Mapping in Various Areas of the Easternmost Mediterranean Based on an Integrated Geological-geophysical Analysis. *In*: (Eppelbaum L., Ed.), *New Developments in Paleomagnetism Research,* Ser: Earth Sciences in the 21st Century, Nova Science Publisher, NY, 15-52.

Eppelbaum, L.V. and Khesin, B.E., 2012. *Geophysical Studies in the Caucasus*. Springer, Heidelberg –N.Y. –London.

Eppelbaum, L.V., Kutasov, I.M. and Pilchin, A.N., 2014. *Applied Geothermics*. Springer, Heidelberg – N.Y. – London.

Gadjiyev, R.M., 1965. *Deep Geologic Structure of Azerbaijan*. Azerneshr, Baku (in Russian).

Gadjiev, T.G., Nechayev, Yu.V., Potapova, E.I., and Sattarova, V.M., 1989. *The Map of Deep Structure of the Caucasus According to Cosmic Data*. Map Printing Factory of the Ministry of Geology of the USSR, Moscow.

Gasanov, A.G., 2001. *Deep Structure and Seismicity of Azerbaijan in Relation to Hydrocarbons Prognosis*. Elm, Baku (in Russian).

Gorodnitsky, A.M., Zonenshain, L.P. and Mirlin, E.G., 1978. *Reconstructions of the Continents in Phanerozoic*. Nauka, Moscow (in Russian).

Gorshkov, A.I. and Niauri, G.A., 1984. Reflection of fault tectonics of the Caucasus in zones of horizontal gravity anomaly gradients. *Izvestiya*, *Acad. Sci. USSR, Physics of the Earth*, **20**, No. 9, 699-704 (in Russian).

Gravity map of the USSR, 1990. Scale 1:2,500,000, Ministry of Geology. Moscow.

Hartley, R.V.L., 1942. A more symmetrical Fourier analysis applied to transmission problems. *Proc. IRE*, **30**, No. 2, 144-150.

Ismailzadeh, A. D., Mustafayev, G. V., & Rustamov, M. I. (Ak. A. Alizadeh, Ed.). (2005). Geology of Azerbaijan, Magmatism (Vol. III). Nafta-Press, Baku (in Russian)

Issayeva, M.I. and Khalafly, A.A., 2006. Paleomagnetic Studies of the Caucasian Segment of the Alpine Fold Belt. *In:* (Ismailzadeh, A.T., Ed.)*, Proceedings of the International Workshop on Recent geodynamics, Georisk and Sustainable Development in the Black Sea to Caspian Sea Region* (Baku, 2005), American Inst. of Physics, Melville, N.Y., 132-135.

Kaban, N.K., 2000. Gravity model of lithosphere and geodynamics. In: *Recent Tectonics, Geodynamics and Seismicity of the Northern Eurasia*. Probel, Moscow, 267-290 (in Russian).

Kadirov, F.A., 1998. Geological interpretation of full horizontal gradients of the gravity field in Azerbaijan. *Izvestiya, Acad. Sci. Azerb*, Ser.: Earth Sciences, No. 5-6, 129-134 (in Russian).

Kadirov, F.A., 2000a. *Gravity Field and Models of Deep Structure of Azerbaijan*. Nafta-Press, Baku (in Russian).

Kadirov, F.A., 2000b. Application of the Hartley transform for interpretation of gravity anomalies in the Shamakhy–Gobustan and Absheron oil- and gas-bearing regions, Azerbaijan. *Jour. of Applied Geophysics*, **45**, 49-61.

Kadirov, F.A., 2004. Gravity models of lithosphere in the Caucasus – Caspian region. In: (Alizade, Ak.A., Ed.), *South Caspian Basin: Geology, Geophysics, Oil and Gas Content.* Nafta-Press, Baku, 107-122.

Kadirov, F.A. and Gadirov, A.H., 2014. A gravity model of the deep structure of South Caspian Basin along submeridional profile Alborz–Absheron Sill. *Global and Planetary Change*, **114**, 66-74.

Kadirov, F.A., Mammadov, S.A., Reilinger, R. and McClusky, S., 2008. Some new data on modern tectonic deformation and active faulting in Azerbaijan (according to Global Positioning System Measurements). *Izvestiya, Acad. Sci. Azerb*., Ser.: Earth Sciences, No. 1, 82-88.

Kerimov, K.M., Pilchin, A.N., Gadjiev, T.G. and Buachidze, G.Y., 1989. *Geothermal map of the Caucasus, Scale* 1:1,000,000 Baku, Cartographic Plant No. 11 (in Russian).

Khain, V.E. and Ryabukhin, A.G., 2002. Russian geology and the plate tectonics revolution. *Geological Society*, *Special Publications*, London, **192**, 185-198.

Khesin, B.E., Alexeyev, V.V. and Eppelbaum, L.V., 1993. 3-D modeling of gravity and magnetic fields as a final stage of application of effective interpretation system of geophysical data under difficult geological conditions. *Geoinformatics*, **4**, No.3, 177-188.

Khesin, B.E., Alexeyev, V.V. and Eppelbaum, L.V., 1996. *Interpretation of Geophysical Fields in Complicated Environments*. Kluwer Academic Publishers, *Ser.: Modern Approaches in Geophysics*, Dordrecht – Boston - London.

Khesin, B.E., Alexeyev, V.V. and Metaxa, Kh.P., 1983. *Interpretation of Magnetic Anomalies in the Conditions of Oblique Magnetization and Rugged Topography*. Nedra, Moscow (in Russian).

Klushin, I.G. and Tolstikhin, I.N., 1961. Singling out linear tectonic dislocations in geophysical maps. *Geology and Geophysics*, No.6, 98-103 (in Russian).

Kopf, A. Deyhle, A., Lavrushin, V.Y., Polyak, B.G., Gieskes, J.M., Buachidze, G.I., Wallmann, K., and Eisenhauer, A., 2003. Isotopic evidence (He, B, C) for deep fluid and mud mobilization from mud volcanoes in the Caucasus continental collision zone. *Intern. Jour. of Earth Sciences*, **92**, 407-425.

Kulhanek, O., 1976. *Introduction to Digital Filtering in Geophysics*. Elsevier, Amsterdam.

Kunin, N.Ya., 1968. Problems of singling out the observed gravity field components for structural-tectonic regioning (as applied to the Southern Kazakhstan), *In: Geophysical investigations in Kazakhstan*. Kazakh. Geoph. Inst., Alma-Ata, 76-88 (in Russian).

Lebedev, L.I. and Tomara, G.A., 1981. Some peculiarities of distribution of heat flow in the South Caspian. In: *Geothermometers and Paleotemperature Gradients*. Nauka, Moscow, 156-161 (in Russian).

Lodzhevsky, M.I. and Kadirov, F.A., 2001. *Caspian Region: Bouguer Gravimetry Map*. Scale 1:1,000,000. Fedynsky Centre GEON & Geol. Inst. of the Azerb. Acad. of Sci.

Mamedov, P.Z., Guliyev, Q.Q., Kadirov, F.A., Shikhalyev, Y.A., Guliyev, I.S., Aliyeva, E.H., Feyzullayev, A.A., Dadashov, F.Q., Kheirov, M.B. and Tagiyev, M.F., 2008. (Ak.A. Alizadeh, Ed.), 2008. *Geology of Azerbaijan*, Vol. VII: *Oil and Gas*. Nafta-Press, Baku (in Russian).

Mekhtiyev, S.F., Mirzadjanzade, A.H. and Aliyev, S.A., 1971. *Geothermal Studies of Oil and Gas Fields*. Nedra, Moscow (in Rissian).

Mekhtiyev, S.F., Mirzadjanzade, A.H., Aliyev, S.A. et al., 1960. *Thermal Regime of Oil and Gas Fields*. Azerneftneshr, Baku (in Russian).

Mekhtiyev, S.F., Hasanov, F.D. and Mukhtarov, A.Sh., 2003. Radiogenic heat generation and heat flow in the South-Caspian Basin. *Bilgi,* No. 3, 99-105 (in Russian).

Mukhtarov, A.Sh., 2004. Heat flow distribution and some aspects of thermal field formation in the Caspian region. In: (Ak. A. Alizadeh, Ed.), *South Caspian Basin: Geology, Geophysics, Oil and Gas Content*. Nafta-Press, Baku, 165-172.

Mukhtarov, A.Sh., 2011. Structure of thermal flow of sedimentary complex of the Southern Caspian Basin. *D.Sci. Thesis*, Inst. of Geology, Baku (in Russian).

Mukhtarov, A.Sh., 2012. Models of distribution of temperatures in sedimentary section of the South Caspian Basin. In: (Ak.A. Alizadeh, Ed.), *Modern Problems of Geology and Geophysics of the Caucasus*. Nafta-Press, Baku, 214-230.

Nikolsky, Yu.I., Milai, T.A. and Kogan, L.Z., 1975. *Geological-Geophysical Studies of the Tectonics, Magmatism, and Metallogeny of the Caucasus*. Nedra, Leningrad (in Russian).

Paffenholtz, K.A., 1959. *Geological Essay of the Caucasus*. Acad. of Sci. of Arm. SSR, Yerevan (in Russian).

Pavlenkova, G.A., 2012. Structure of the Caucasus' earth crust along the deep seismic sounding profiles Stepnoe-Bakuriani and Volgograd-Nakhchivan (results of initial data re-interpretation). *Izvestiya*, *Physics of the Earth*, No. 5, 16-25.

Peyve, A.V., Zonenshayn, L.V., Knipper, A.L. et al., 1980. *Tectonics of the Northern Eurasia. Explanation Notes to Tectonic Map of the Northern Eurasia, Scale 1:5,000,000.* Nauka, Moscow (in Russian).

Pilchin, A.N. and Eppelbaum, L.V., 1997. Determination of magnetized bodies lower edges by using geothermal data. *Geophysical Journal International*, **128**, No.1, 167-174.

Radjabov, M.M., 1978. Study of the structure of the earth's crust-consolidated complex of the Azerbaijan using deep seismic sounding and refracted wave-correlation method data. In: *The Structure of the Earth's Crust and Upper Mantle in the Central and East Europe*. Naukova Dumka, Kiev, 205-211 (in Russian).

Reilinger, R., McClusky, S., Vernant, P. Lawrence, S., Ergintav, S., Cakmak, R., Ozener, H., Kadirov, F., Guliyev, I., Stepanyan, R., Nadariya, M., Hahubia, G., Mahmoud, S., Sakr, K., ArRajehi, A., Paradissis, D., Al-Aydrus, A., Prilepin, M., Guseva, T., Evren, E., Dmitrotsa, A., Filikov, V., Gomez, F., Al-Ghazzi, R. and Karam, G., 2006. GPS constraints on continental deformation in the Africa-Arabia-Eurasia continental collision zone and implications for the dynamics of plate interactions. *Jour of Geophysical Research,* **111**, B05411, 1-26.

Riznichenko, Yu.V., Khesin, B.E. and Metaxa, Kh.P., 1983. Relation between seismicity and magnetic field according to observations in Azerbaijan. *Izvestiya*, *Acad. Sci. Russ.,* Ser.: Physics of the Solid Earth, No.1, 3-14 (in Russian).

Rustamov, R.I., 2001. Geothermal regime of the South Caspian Sea region. *Azerbaijan Oil Industry,* Nos. 4-5, 28-32 (in Russian).

Sandwell, D.T., Garcia, E., Soofi, K., Wessel, P. and Smith, W.H.F., 2013. Towards 1 mGal Global Marine Gravity from CryoSat-2, Envisat, and Jason-1. *The Leading Edge*, **32**, No. 8, 892-899.

Sandwell, D.T. and Smith, W.H.F., 2009. Global marine gravity from retracked Geosat and ERS-1 altimetry: Ridge Segmentation versus spreading rate. *Journal of Geophysical Research*, **114**, B01411, 1-18.

Sirotkina, T.N. and Nikolsky, Yu.I., 1971. Method of successive geological approximations by interpretation of geophysical fields in ore regions (on example of Armenia). *Methods of Exploration Geophysics,* No. 12, 36-44 (in Russian).

Somerton, W.H., 1992. *Thermal Properties and Temperature Related Behavior of Rock/Fluid Systems*. Developments in Petroleum Science, **37**. Elsevier, Amsterdam.

Spector, A. and Grant, F.S., 1970. Statistical models for interpreting aeromagnetic data. *Geophysics*, **35**, 293-302.

Shengelaya, G.Sh., 1984. *Gravity Models of the Caucasus' Earth crust*. Nauka, Moscow (in Russian).

Shikhalibeyli, E.Sh., 1996. *Some Problems of Geological Structure and Tectonics in Azerbaijan*. Elm, Baku (in Russian).

Sukharev, G.M., Taranukha, Y.K. and Vlasova, S.P., 1969. Thermal flow from Azerbaijan subsoil. *Soviet Geology,* No. 8, 146-153 (in Russian).

Sundararajan, N., 1995. 2-D Hartley transforms. *Geophysics*, **60**, 262-265.

Tauxe, L., Banerjee, S.K., Butler, R. F. and van der Voo, R., 2009. *Essentials of Paleomagnetism*: *Web Edition*. http://magician.ucsd.edu/essentials/WebBook.html

Tikhonov, A.N. and Bulanzhe, Yu.D., 1945. On the gravity field averaging. *Izvestiya, Ser. Geoph.*, USSR Acad. Sci., No 2 (in Russian).

Vinnik, L.P., 1976. *Investigations of the Earth's Mantle by Seismic Methods*. Nauka, Moscow (in Russian).

Yaglom, A.M. and Yaglom, I.M., 1973. *The probability and Information*. 2nd ed., revised and supplemented. Nauka, Moscow (in Russian).

Yakubov, A.A. and Atakishiyev, I.S., 1973. *Geothermal Studies of Oil and Gas Fields of Absheron*. Azerneshr, Baku (in Russian).

Zeynalov, G.A., 2000. Importance of remote-sensing data in structural geologic analysis of oil-and gas bearing regions of Azerbaijan. *Natural Resources Research*, **9**, No. 4, 307-313.

Zolotovitskaya, T.A., 2003. Mechanisms of formation of radionuclide contamination at the oil fields of Azerbaijan. *In*: (N. Birsen, and K. K. Kadyrzhanov, Eds.), *Environmental protection against radioactive pollution*. Kluwer Acad. Publ., NATO Science Series, Earth & Environmental Sci., Vol. **33**, 74-77.